Geological Society of America Bulletin, published online on 1 February 2016 as doi:10.1130/B31431.1

Dynamic topography and vertical motion of the U.S. Rocky Mountain region prior to and during the Laramide orogeny

Paul L. Heller[1,†] and Lijun Liu[2]
[1]*Department of Geology and Geophysics, University of Wyoming, Laramie, Wyoming 82071, USA*
[2]*Department of Geology, University of Illinois at Urbana-Champaign, Champaign, Illinois 61820, USA*

ABSTRACT

Dynamic topography of Earth's surface occurs in response to hydrodynamic stresses due to mantle flow beneath a flexible lithosphere. Here, we compare the predicted dynamic topography from an inverse-convection model that includes flat slab subduction with the known geologic history of the western United States from Late Cretaceous through Paleocene time to evaluate the validity of the model results. Downwarping behind the evolving Cordilleran volcanic arc took place after its inception in Late Triassic time, culminating in the formation of the Western Interior Seaway in Late Cretaceous time. Subsidence behind arcs is a consistent prediction of most models of dynamic topography. A more-detailed convection model is evaluated here by comparing it to the geologic history of the central Rocky Mountain region from 100 to 50 Ma. The match of predicted and observed tectonic subsidence is good up until the time that local deformation by the Laramide orogeny begins. This is most likely due to local flexural effects of mountain building overwhelming regional dynamic effects.

Maps for successive time intervals show that the model matches the geologic history quite well through time and space; in particular, the subduction of the previously postulated oceanic plateau—the conjugate Shatsky Rise—has a significant impact on surface movements. (1) From 95 to 88 Ma, the locations of most significant regional unconformities match the eastward migration of a zone of high topography. (2) From 90 to 85 Ma, the zone of maximum subsidence coincides with the motion of the leading edge of the conjugate Shatsky Rise. (3) From 78 to 60 Ma, the site of initiation of Laramide deformation migrates coincidently with the position of the center of the conjugate Shatsky Rise. (4) From 70 to 60 Ma, the time-transgressive deposition of thin fluvial conglomerate units in the southern part of the study area is generally coincident with surface uplift caused by the trailing part of the conjugate Shatsky Rise. These results suggest that the inverse model approximates the vertical motion history quite well.

Synchroneity of the position of the center of the passing conjugate Shatsky Rise, the landward limit of the evolving Cordilleran volcanic arc, and the initiation of Laramide deformation suggests that the Farallon plate became coupled with the overlying North American plate as the subducted oceanic plateau passed beneath. Progressively enhanced mechanical coupling between the plates was likely the impetus for Laramide shortening. This comparison of model results with surface geologic history provides a means to validate, but not verify, predictions of dynamic mantle-flow models.

INTRODUCTION

Dynamic topography is the vertical deflection of Earth's surface caused by hydrodynamic stresses generated by sublithospheric mantle flow. While such deflections must occur on a flexible earth, their amplitudes need not be very large. Typical calculated deflections reach amplitudes on the scale of 1 km and wavelengths of many hundreds of kilometers. Dynamic topography has been used to interpret the origins of some large-scale uplift and subsidence patterns found on Earth today and in the past (Gurnis, 1993; Lithgow-Bertelloni and Silver, 1998). These patterns are seen in the ancient record by subsidence analysis, continental flooding history, isopach patterns, thermochronology, and reconstruction of continental tilting (Bond, 1976; Mitrovica et al., 1989; Smith et al., 1994; Heller et al., 2003; Flowers et al., 2008; Painter and Carrapa, 2013; Liu et al., 2014). In cases where there have been past surface deflections of large subcontinental scale in places far from areas of known tectonism, dynamic topography must be considered as a potential cause. While not all deflections must have a dynamic origin, those regions most likely to have been affected by dynamic topography will include a broad-wavelength, low-amplitude deflection that is necessarily transient in time at plate-tectonic rates.

While different models of dynamic topography seem to agree at long wavelengths (>1000 km), they can significantly depart in detail (Braun, 2010; Flament et al., 2013). This is due to the many uncertainties in solid-earth parameters that affect model results, such as rheologic behavior of the mantle, thermal structure, density profiles, and the past history of mantle-surface interactions (Flament et al., 2013; Liu, 2015). One way to evaluate such models is by comparison with regional geologic history (Gurnis et al., 1998). The goal of this paper is to compare predictions from one such model, that of Liu et al. (2008), with the history of vertical motions in a relatively well-understood region—in this case, the history of the U.S. Rocky Mountains between 100 and 50 Ma. In doing so, we hope to isolate surface topography generated by tectonic effects from those due to mantle convection.

DYNAMIC TOPOGRAPHY

Dynamic topography refers to the surface manifestation of sublithospheric vertical stress generated from buoyancy-driven mantle flow. In general, downward sublithosphere mantle flow (downwelling) leads to dynamic subsidence, and upwelling leads to dynamic uplift. In observation, dynamic topography differs from its isostatic counterpart (flexural topography included) in its spatial and temporal characteristics (Liu, 2015). Three unique properties may help to distinguish dynamic topography from topography generated by isostatic effects. (1) Because of the

[†]heller@uwyo.edu

 doi: 10.1130/B31431.1; 8 figures; 1 table; Data Repository item 2016042.

Geological Society of America Bulletin, published online on 1 February 2016 as doi:10.1130/B31431.1

highly viscous nature of Earth's interior, mantle flow–induced stresses can translate over large distances. As a result, mantle flow usually occurs over large spatial scales (>200 km), as does the resulting surface dynamic topography. (2) The magnitude of dynamic topography is limited to ~1 km or less, due to strong viscous dissipation and redistribution of localized mantle buoyancy force over large spatial extents. (3) Dynamic topography evolves at a rate comparable to tectonic plate motions.

In theory, the most fundamental difference between isostatic and dynamic topography is the source of driving forces. Isostatic topography usually originates from buoyancy heterogeneities from within the strong lithosphere through either lateral density or thickness variation (Fig. 1A). Due to its shallow compensation depth, isostatic topography has a weak gravity signature at long wavelengths. Dynamic topography, in contrast, is associated with the viscous stress in the sublithospheric mantle, where the stress originates from buoyancy-driven flow (Fig. 1B). Thus, induced dynamic topography is usually poorly compensated by shallow density structures, leaving a large gravity/geoid signal at the surface (Hager, 1984).

Models of mantle convection with the purpose of estimating dynamic topography show a trend of convergence on long-wavelength predictions, especially in regions involving subduction processes. For example, broad depression of the land surface occurs in response to active or former subduction, as seen from modeling of continental flooding and ocean basin subsidence (Mitrovica et al., 1989; Gurnis, 1993; Liu et al., 2008; Flament et al., 2014). At larger scales, regions inboard of volcanic arcs tend to dynamically subside (e.g., Billen and Gurnis, 2003), but uplift can result if strong lateral compression within the overriding plate occurs (Capitanio et al., 2011). More debates exist on the predictions of dynamic topography for areas away from active subduction zones, where the various uncertainties would influence dynamic topography calculations.

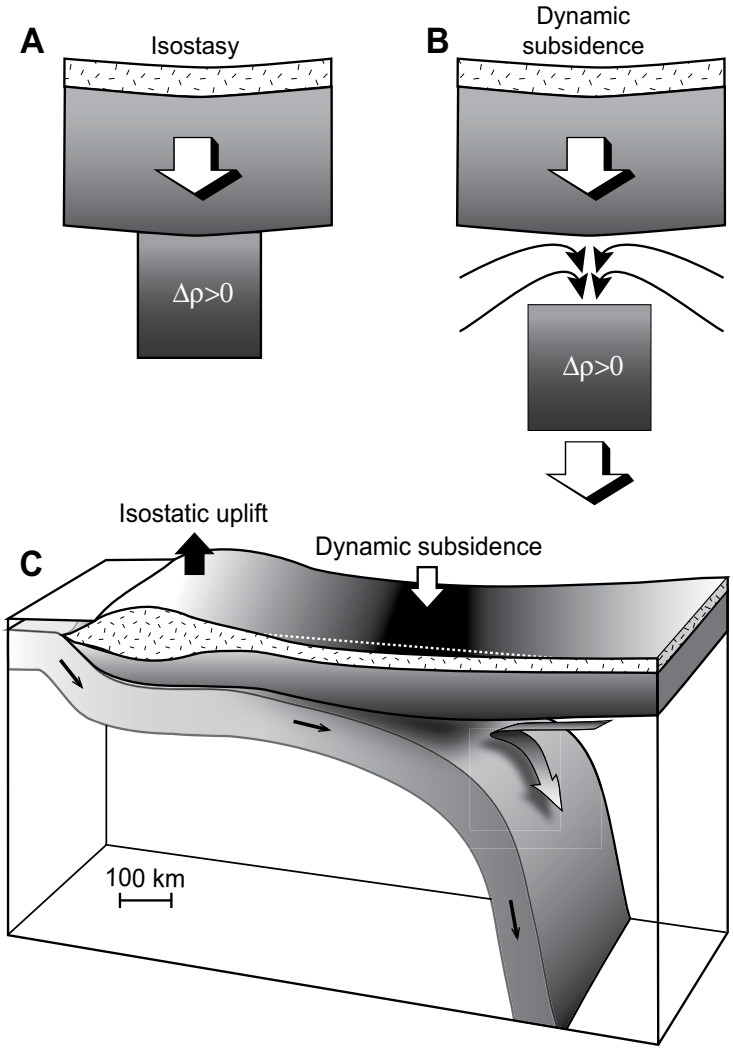

Figure 1. Diagrams illustrating the differences between (A) isostatic and (B) dynamic subsidence mechanisms as discussed in text. In A, additional dense mantle lithosphere (Δρ > 0, shaded) is attached to upper plate, causing surface deflection by flexure. In B, a block of mantle material is sinking through the asthenosphere, causing downwelling of the overlying mantle wedge and generating downward stresses on the overlying plate. (C) Dynamic subsidence generated by subduction and associated mantle flow (large arrow).

The inverse mantle-convection model of Liu et al. (2008) adopts an adjoint inversion method in order to reconstruct the past mantle structures from present-day mantle seismic images. The model assumes that the observed fast seismic velocities beneath eastern North America can convert to an effective temperature structure, i.e., density anomalies. The model includes the presence of the U.S. Western Interior Seaway of Late Cretaceous age as a constraint on the predicted history of the surface deflection of North America. Here, we take the predictions of this model and compare them in greater detail to the history of part of the U.S. Cordillera for the period from Late Cretaceous to Paleogene time (100–50 Ma) in order to validate the model results. To the degree that the model fits the known geologic history, insight is provided into the coupling between the North American and Farallon plate over the period during which the Laramide orogeny affected the Rocky Mountains.

Based on both the inverse model and a kinematic restoration of western Pacific oceanic plateaus, Liu et al. (2010) proposed that the conjugate plateau of the Shatsky Rise subducted beneath the western United States, causing the Farallon plate to subduct as a low-angle, flat slab during Late Cretaceous time (Saleeby, 2003). Interaction of the flat slab around the downgoing conjugate Shatsky Rise with the overriding North American lithosphere generated the maximum surface deflections in the model of Liu et al. (2008).

MESOZOIC MIGRATORY SUBSIDENCE

A first-order response seen in most models of dynamic topography is a general subsidence pattern in areas inboard of subduction zones (Fig. 1C). The flatter is the subducted slab, the broader is the area of subsidence. This response

Geological Society of America Bulletin, published online on 1 February 2016 as doi:10.1130/B31431.1

was manifested in the U.S. Cordillera from the onset of Andean-type subduction in Late Triassic time (Armstrong and Ward, 1993) through at least Cretaceous time. Sedimentation patterns show evidence of downward deflection immediately east of the evolving continental volcanic arc throughout Mesozoic time (Fig. 2). Low areas were manifested by depositional centers in Late Triassic and Early Jurassic time, marine incursions during Middle Jurassic and Late Cretaceous time, and broad dispersal patterns in fluvial systems during Late Jurassic and Early Cretaceous times (Fig. 2, and references therein). The center of subsidence migrated eastward throughout the Mesozoic as eastward subduction continued and the position of the continental arc expanded over time. Of course, these depocenters could have had other driving mechanisms, such as localized flexural subsidence or preexisting regional topography, exerting primary control (Blakey et al., 1988; Bjerrum and Dorsey, 1995; Allen et al., 2000). However, the eastward migration of the depositional centers, their broad wavelength, and their generally low amplitude suggest that dynamic topography likely played an important role (Mitrovica et al., 1989; Lawton, 1994; Allen et al., 2000; Heller et al., 2003).

MIDDLE CRETACEOUS TO EOCENE RECORD OF SUBSIDENCE AND UPLIFT

A more detailed comparison between the results of the model of Liu et al. (2008) and the history of the Rocky Mountains can be done for the period of 100 to 50 Ma, the period during which the purported conjugate Shatsky Rise passed beneath the region (Saleeby, 2003; Liu et al., 2010). During this period, the region underwent shortening. The Sevier orogeny, a retroarc fold-and-thrust belt found west of the study area (Fig. 3), began during Early Cretaceous time and continued until ca. 50 Ma (DeCelles, 2004; Yonkee and Weil, 2015). During the Laramide orogeny (Late Cretaceous–middle Eocene; Dickinson et al., 1988), shortening deformation stepped to the east as basement-cored uplifts that form most of the present ranges of the Rocky Mountains. The shift of the locus of shortening between the Sevier and Laramide orogenies can be viewed as a continuation of eastward deformation of the Cordilleran orogenic wedge (DeCelles, 2004). However, differences in shortening direction between the two orogenic belts suggest that the two events may have different, if not related, driving mechanisms (Erslev, 1993; Bird, 1998).

The timing of onset of the Laramide orogeny has not been well established. Dickinson et al. (1988) compiled syntectonic sedimentary data from Rocky Mountain basins to argue that deformation began everywhere in Maastrichtian time at 70 ± 5 Ma. Others have suggested that Laramide deformation began earlier, from 80 to 75 Ma (DeCelles, 2004), or even earlier (Schwartz and DeCelles, 1988; Steidtmann and Middleton, 1991). In either case, the driving force for the Laramide orogeny is widely viewed to have been related to flat slab subduction of the Farallon plate beneath North America and basal traction caused by coupling between the plates (Dickinson and Snyder, 1978; Bird, 1998). Primary evidence for this interpretation came from the coincidence of Laramide timing with migration of the Cordilleran magmatic arc (Coney and Reynolds, 1977; Dickinson and Snyder, 1978). Interpretations of the driving force of flat slab subduction include increased plate convergence rates (Coney and Reynolds, 1977; Coney, 1978), and/or increased buoyancy of the Farallon plate by either decreasing age (Engebretson et al., 1985) or subduction of a buoyant oceanic plateau (Livaccari et al., 1981; Saleeby, 2003).

Migration of a flat slab coupled to North America would be expected to cause localized migratory shortening in the overlying plate (Bird, 1998). Alternatively, Laramide deformation could have resulted from stresses generated by increased viscous shear coupling across the subduction zone. These stresses would then be transmitted inboard across the North Amer-

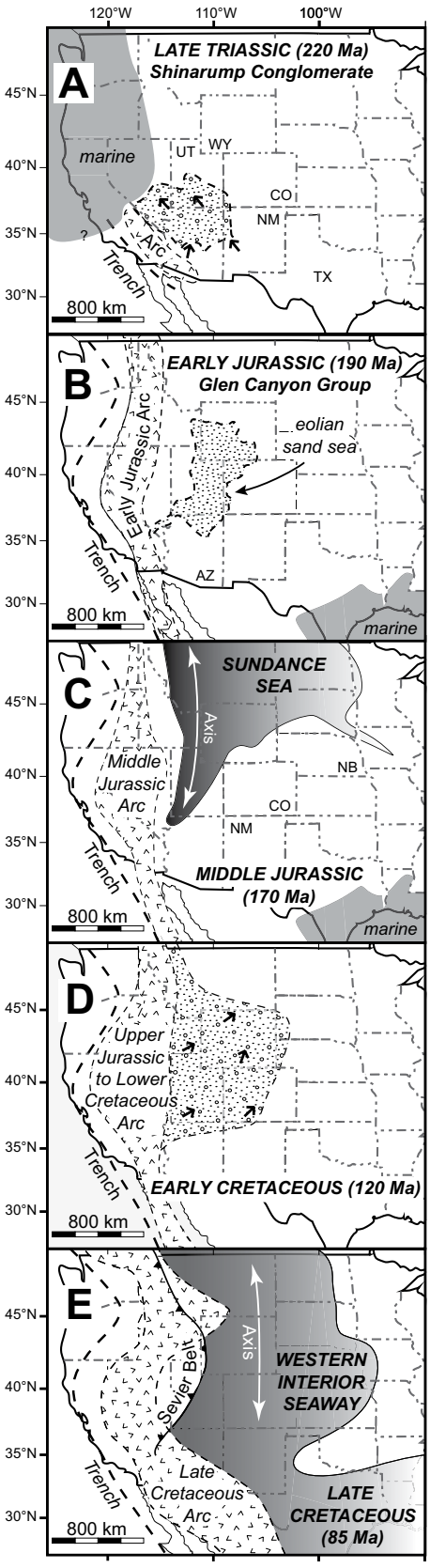

Figure 2. Maps of western United States showing position of the continental arc and evidence of retroarc subsidence, which may have been partially controlled by dynamic topography associated with subduction of the Farallon plate beneath North America. Arc positions were taken from North American Volcanic and Intrusive Rock Database (NAVDAT data, http://www.navdat.org). (A) Late Triassic, showing paleogeography of the Shinarump Conglomerate Member of the Chinle Formation (from Heller et al., 2003). (B) Early Jurassic distribution of Glen Canyon Group eolian deposits (after McKee, 1988). (C) Middle Jurassic Sundance seaway (after Peterson, 1972). (D) Early Cretaceous fluvial conglomerate deposits (from Heller et al., 2003). (E) Late Cretaceous Western Interior Seaway (from Heller et al., 2003). State abbreviations: UT—Utah, WY—Wyoming, CO—Colorado, NM—New Mexico, TX—Texas, AZ—Arizona, NB—Nebraska.

Geological Society of America Bulletin, published online on 1 February 2016 as doi:10.1130/B31431.1

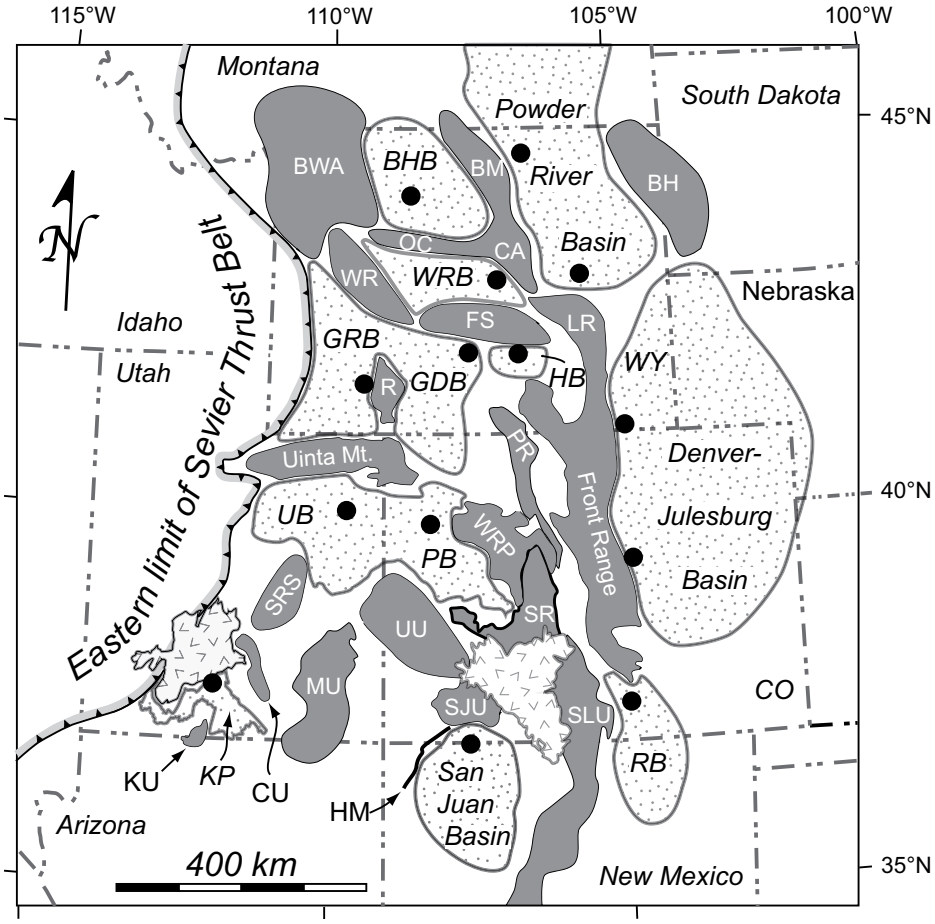

Figure 3. Base map of uplifts and basins in the Rocky Mountains and locations used for subsidence analysis. Basins: BHB—Bighorn Basin; GDB—Great Divide Basin; GRB—Green River Basin; HB—Hanna Basin; KP—Kaiparowits Plateau; PB—Piceance Creek Basin; RB—Raton Basin; UB—Uinta Basin; WRB—Wind River Basin. Uplifts: BH—Black Hills; BM—Bighorn Mountains; CA—Casper Arch; BWA—Beartooth–Washakie-Absaroka Ranges; CU—Circle uplift; FS—Ferris, Green, Seminoe, Shirley Mountains; HM—Hogback Monocline; KU—Kaibab uplift; LR—Laramie Range; MU—Monument upwarp; OC—Owl Creek Mountains; PR—Park Range; R—Rock Springs uplift; SJU—San Juan uplift; SLU—San Luis uplift; SR—Sawatch Range; SRS—San Rafael Swell; UU—Uncompahgre uplift; WR—Wind River Range; WRP—White River Plateau. State abbreviations: CO—Colorado, WY—Wyoming.

ican plate. This end-loading, whether caused by collision of a crustal block or an increase in relative velocity between the Farallon and North American plates (Livaccari and Perry, 1993; Maxson and Tikoff, 1996; Tikoff and Maxson, 2001), would have led to increased compression across the entire upper plate at the same time. Such predicted synchronicity is consistent with the results of Dickinson et al. (1988), which show that the Laramide orogeny began at more-or-less the same time across the Rockies. Therefore, reconsideration of the timing of initiation of the Laramide orogeny may help to clarify which of these driving forces dominated.

Conjugate Shatsky Rise

The oceanic plateau model for the origin of the Laramide orogeny is based upon plate reconstructions that suggest the Shatsky Rise in the Pacific Basin formed along a spreading center beginning in Late Jurassic–Early Cretaceous time (Smith, 2007). If so, then mirror oceanic plateaus would very likely have formed on both sides of the spreading center, just as seen in the analogous case of the formation of Iceland today along the Mid-Atlantic Ridge (Lawver and Müller, 1994). With continued plate spreading, the plateaus on the Farallon plate, the conjugate Shatsky Rise, would have eventually collided with North America in the vicinity of southern California sometime between 90 and 85 Ma (Saleeby, 2003). As the Farallon plate subducted under North America, so too would have the attached conjugate Shatsky Rise.

The dynamic effect of the migrating conjugate Shatsky Rise on the overlying North American plate would have changed over time. During the initial collision, and soon thereafter, the thickened crust of the Farallon plate was a buoyant topographic high due to isostatic compensation, promoting direct contact and coupling with the overlying plate. This facilitated tectonic erosion of North America in southern California during Late Cretaceous time (Saleeby, 2003) and likely caused isostatic uplift and exhumation of the broad region encompassing the southern Sierra Nevada Batholith (Saleeby et al., 2007). Farther inboard, the Farallon slab sank to greater depths, during which the mechanical interaction between the two plates would have switched from direct contact to a hydrodynamic coupling, with the transition depth dependent upon the thickness of the overriding plate. In effect, the strong coupling via shearing deformation between the subducting slab and the overriding plate transmitted much of the negative buoyancy of the slab to the surface, leading to widespread subsidence in the western United States.

Meanwhile, the negative buoyancy of the flat slab would gradually have increased due to eclogitization of the basaltic crust, a well-understood process in specific laboratory experiments (Aoki and Takahashi, 2004; Xu et al., 2008) but poorly constrained when applied to real tectonic scenarios due to uncertainties in rock composition and thermal states. Part of the debate on dynamic topography associated with oceanic plateau subduction (cf. Liu and Gurnis, 2010; Dávila and Lithgow-Bertelloni, 2015) comes from differing assumptions regarding basalt-eclogite phase transformation within the downgoing plate. Liu et al. (2010) assumed that the thickest part of the inverted flat slab correlates exactly with the conjugate Shatsky Rise, which is consistent with its reconstructed position and time of arrival in their plate reconstruction. However, an outstanding question remains as to whether the slab flattening was caused purely by the positive buoyancy of the plateau crust or by the hydrodynamic suction from the thick overriding plate as well (Taramón et al., 2015). If the latter mechanism played an important role, we would not necessarily expect a perfect spatial correlation between the flat slab and the conjugate Shatsky Rise.

During Farallon flat subduction, the magnitude of dynamic coupling and, thus, downward

Geological Society of America Bulletin, published online on 1 February 2016 as doi:10.1130/B31431.1

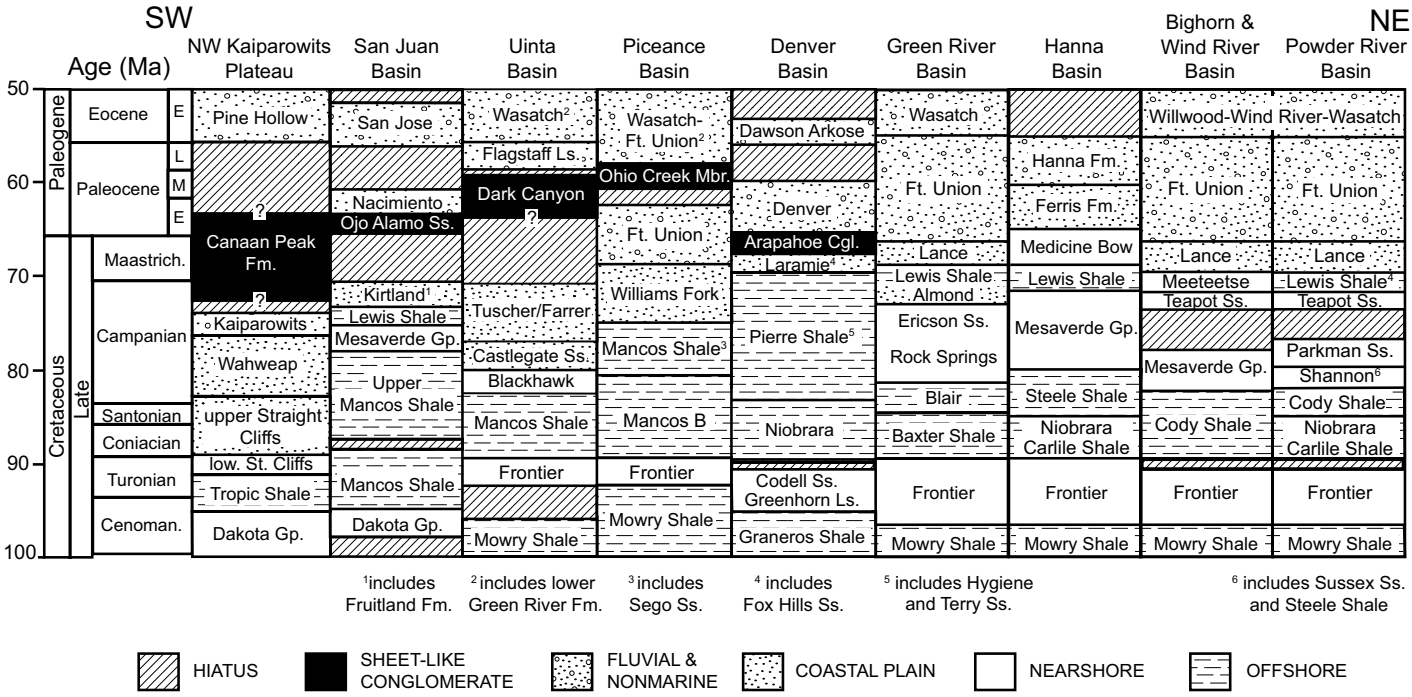

Figure 4. Stratigraphic correlation of units involved in this study in Rocky Mountain basins. General stratigraphy and age data were summarized in Cobban and Reeside (1952); Merewether and Cobban (1986); Kauffman et al. (1993); Heller et al. (2013); and Wyoming Geological Association Stratigraphic Committee (2014). Other references on stratigraphy, age control, lithofacies, and depositional environment are listed in Appendix A (see text footnote 1). Time scale is from Gradstein et al. (2012). Cgl—conglomerate, Ss—Sandstone, Ls—Limestone, Gp—Group, Fm—Formation.

pull would be greatest above the leading part of the flat slab, especially as the basaltic crust of the conjugate Shatsky Rise turned to eclogite. This is because, first, the elevated surface of the flat slab would reduce the thickness of the overlying mantle wedge, leading to higher dynamic suction (Fig. 1C; Stevenson and Turner, 1977; Manea and Gurnis, 2007). Second, the more steeply dipping slab in front of the flat slab would induce a strong downwelling, increasing dynamic subsidence. As the flat slab migrated to the northeast, so too would the center of maximum subsidence. At the same time, the magnitude of subsidence would decrease as the slab was subducted to greater depths. By ca. 50 Ma, the flat slab moved beyond the Rocky Mountain region. As the wave of subsidence migrated, surface topography rebounded in its wake (Liu et al., 2010).

METHODS

Our specific goal was to compare the dynamic topography predictions from the adjoint inverse model of Liu et al. (2010) with the records of tectonic timing of the Laramide orogeny and the history of basin subsidence for Rocky Mountain basins (Fig. 3).

Subsidence History

Vertical motions in each of the basins shown on Figure 3 were interpreted here by subsidence analysis using stratigraphic sections derived primarily from wells. These subsidence curves have been backstripped, removing subsidence effects due to sediment loading (Steckler and Watts, 1978) and compaction (van Hinte, 1978). Thus, the subsidence history shown is that caused by tectonic processes alone. In some cases, subsidence analyses had already been done (Cather, 2004; Heller et al., 2013). Most of the additional sections used here came from published stratigraphic logs (see Appendix A[1]). In all cases, sections were chosen that had the greatest number of recognized stratigraphic units (Fig. 4). Where well data were used, a second well was evaluated if one could be found close enough to the first well in order to check for consistency of picked stratigraphic horizons. In these cases, for simplicity, only one section is presented here. In the case of the Hanna Basin, multiple measured stratigraphic sections were used to show the uncertainties in picking units where no deep well exists.

Ages were assigned to biostratigraphic units using the Cretaceous Western Interior ammonite time scale of Cobban et al. (2006), with modifications made by Scott (2014), which is tied to the Cretaceous time scale of Gradstein et al. (2012). Tertiary age assignments primarily came from palynology (Nichols and Flores, 1993; Nichols and Fleming, 2002; Nichols, 2003) and land mammal ages (Lillegraven, 1993; Higgins, 2003). Age assignments and stratigraphic correlations are shown in Figure 4.

We used the stratigraphic sections (Appendix A [see footnote 1]) to complete one-dimensional backstripped subsidence analyses following the approach in Angevine et al. (1990). We also used estimates of paleowater depth to approximate uncertainty in the resulting tectonic subsidence curve (Fig. 5). The paleowater depth scale is defined here as inner shelf (0–50 m), middle shelf (50–100 m), outer shelf (100–200 m), upper slope (200–300 m), coastal plain (i.e., fluvial system is tied to a known shoreline; 0 to –50 m), and nonmarine (–50 to –200 m). Water depth assignment was based primarily on lithofacies and sedimentology as described in the literature or, in rare cases,

[1]GSA Data Repository item 2016042, Appendix A, is available at http://www.geosociety.org/pubs/ft2016.htm or by request to editing@geosociety.org.

Geological Society of America Bulletin, published online on 1 February 2016 as doi:10.1130/B31431.1

where indicative benthic fossils have been found (e.g., Martinson et al., 1998). The range of the water depth estimate controls the width of lines on the subsidence curves (Fig. 5). Major hiatuses are shown as gaps in the resulting curves. Minor hiatuses (2 m.y. or less; e.g., Merewether et al., 2007) were ignored, since we were most interested in the overall pattern.

The abrupt, step-like nature of the resulting subsidence curves (Fig. 5) is an artifact of the limited data used to construct the curves. We only included data from the tops and bottoms of identified formations with no control on a finer scale. As such, curve segments are long-term average rates. The real history of subsidence could have changed during the deposition of a formation, but this is not seen in our analysis. For example, a more detailed history from another well in the Denver-Julesburg Basin (Fig. 6) indicates that sediment accumulation rates, a proxy for subsidence, were more episodic and segmented during deposition of the Pierre Shale.

Figure 5 (*on following page*). Tectonic subsidence curves for a middle Cretaceous horizon until early Eocene time (black lines) compared to the range of dynamic topographic model results (gray dashed line) for various basins in the U.S. Rocky Mountains. Indicators of initial or early movement of nearby Laramide uplifts are from Table 1. Width of observed subsidence curve reflects range of paleowater depth. Gaps are major hiatuses. Wells/sections used (Appendix A [see text footnote 1]): (A) Bighorn Basin, Sellers Draw well; (B) northern Powder River Basin, Scales Fee 1-H-10 well; (C) southern Powder River Basin, Kodner W-59968 32–5 well; (D) Great Divide Basin, British American Oil Govt. 1 well; (E) Wind River Basin, Key Spring Unit 1-F14 well; (F) Denver-Julesburg (D-J) Basin, Wyoming, Calco Morton King #1 well; (G) Green River Basin, Dagger Unit 1 well; (H) Hanna Basin, various measured sections; (I) Denver-Julesburg (D-J) Basin, Colorado, combined J.S. Abercrombie State #1 well and the Castle Pines core; (J) Raton Basin, Goemmer #2205 well; (K) Uinta Basin, section 14 of Johnson and Johnson (1991); (L) Piceance Creek Basin, section 35 of Johnson and Johnson (1991); (M) northern Kaiparowits Plateau, field sections; (N) San Juan Basin, Aztec Oil and Gas Trail Canyon No. 1 well. State abbreviations: MT—Montana, ID—Idaho, UT—Utah, WY—Wyoming, CO—Colorado, SD—South Dakota, AZ—Arizona, NB—Nebraska.

Reconstruction of Dynamic Topography

Estimations of past dynamic topography were based on a nonlinear inversion algorithm that solves for an unknown initial condition by iteratively minimizing the mismatch between the predicted present-day mantle structure and the seismically observed one (Liu et al., 2008). The present mantle thermal profile is first converted from a global tomography image (Grand, 2002) using a constant seismic velocity-to-density scaling, during which the uppermost 200 km of fast seismic anomalies are removed, assuming that continental lithospheres are neutrally buoyant and do not contribute to the temporal variation of the surface topography. This buoyancy structure is used as the starting point for the inverse model to retrieve past mantle structures.

Another important constraint on the effective mantle buoyancy and viscosity structure is the presence of the Western Interior Seaway, which requires additional adjustments to the original buoyancy and viscosity estimates in order to reproduce the formation of this feature (Liu and Gurnis, 2008). Reproduction of the overall inundation maps over time and representative subsidence curves from wells within the Western Interior Seaway limit the range of effective mantle buoyancy and viscosity structure (Liu et al., 2008). Apparently, mantle properties thus obtained represent values that are consistent with the large-scale dynamic history of the western United States and global tomography, the spatial resolution of which is not very high (~500 km). The range of model results shown on Figure 5 is based on the permissible mantle properties that fit these constraints (Liu and Gurnis, 2010). The calculated subsidence below sea level assumes isostatic loading by water.

Since the inverse model only solves for the long-wavelength thermal evolution of mantle, it may lack the capability of addressing fine-scale processes, especially those associated with changes in density structure through time, such as would impact the buoyancy of the subducted oceanic plateau (i.e., the conjugate Shatsky Rise). These model limitations suggest that further testing with independent data is necessary in order to better understand regional tectonic processes within the western United States. Given that the Western Interior Seaway was used to constrain the model, it is no surprise to see it reproduced by our results. However, here we are comparing the model results to the regional geologic history at a much finer level. The predicted history of vertical motion at each well is included on the subsidence diagrams of Figure 5, and the predicted dynamic topography maps from the adjoint inverse model are shown in Figure 7.

INITIATION OF LARAMIDE DEFORMATION

One of the goals of this study is to separate subsidence due to mantle dynamics from that caused by flexural subsidence by mountain building during the Laramide orogeny. In the case of the Sevier orogenic belt, discrimination between flexural and dynamic subsidence has been done by predicted subsidence and observed isopach patterns (Liu et al., 2011, 2014; Painter and Carrapa, 2013). Flexural loading produces distinctive, asymmetric subsidence centered under the thrust load, whereas dynamic topography is broad, low-amplitude subsidence not necessarily tied to surface loads. The same approach could be used to identify flexural loading by Laramide uplifts. However, these individual structural uplifts act as relatively small-scale loads that are broadly distributed, and their subsidence patterns can interact in complex three-dimensional patterns, making simple comparison between predicted and observed subsidence patterns difficult. In order to evaluate the timing of local Laramide uplifts, we use evidence independent of subsidence rates. Rapid subsidence events that occurred coincident with these other lines of evidence are then interpreted to be the result of nearby Laramide uplifts and, thus, not solely the result of dynamic topography.

We have compiled evidence for the timing of initiation of Laramide deformation across the Rocky Mountain region (Table 1). We are only concerned with the time of initiation of orogeny because any flexural loading due to mountain uplift would interfere with, and likely overwhelm, vertical motion due to dynamic effects. The record of the Laramide orogeny shows that deformation began slowly in Late Cretaceous time and accelerated in Paleogene time (Bird, 1998). Evidence used in the compilation includes angular unconformities, changes in clastic provenance, shift in paleocurrent directions, isopach patterns showing local asymmetric (flexural) subsidence, fault crosscutting relationships, thermochronologic evidence of rapid unroofing in ranges, introduction of new source areas seen in paleocurrents, and influx of conglomerate in the proximal parts of basins. Of these, the arrival of progradation of conglomerate into basins is mostly likely to be a trailing indicator, as it takes a while for gravels to migrate out into basins (Hoy and Ridgway, 1997; Jones et al., 2004; Leary et al., 2015). The age constraints provided from the stratigraphic

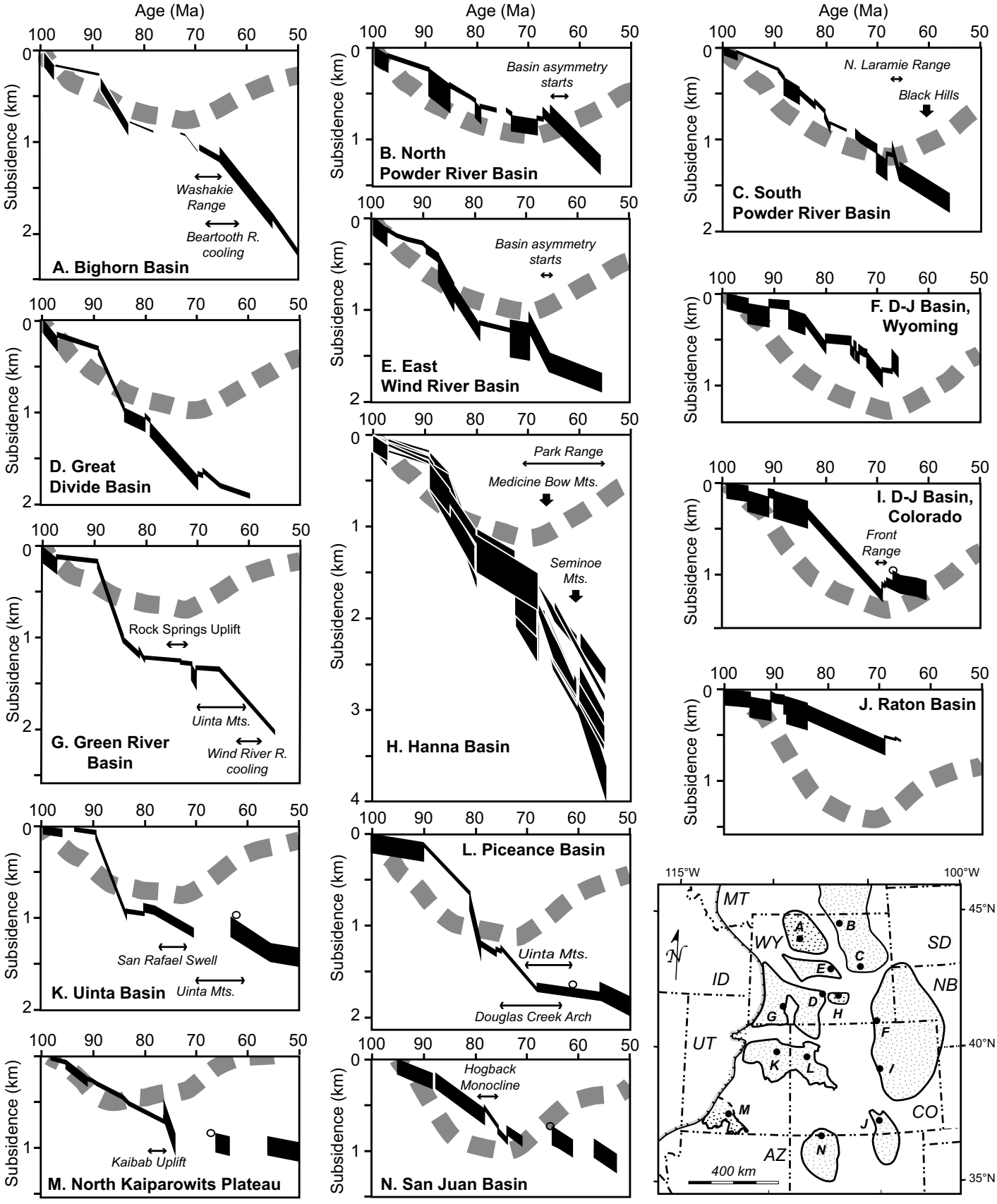
Age (Ma)
Subsidence (km)
A. Bighorn Basin
Washakie Range
Beartooth R. cooling
B. North Powder River Basin
Basin asymmetry starts
C. South Powder River Basin
N. Laramie Range
Black Hills
D. Great Divide Basin
E. East Wind River Basin
F. D-J Basin, Wyoming
G. Green River Basin
Rock Springs Uplift
Uinta Mts.
Wind River R. cooling
H. Hanna Basin
Park Range
Medicine Bow Mts.
Seminoe Mts.
I. D-J Basin, Colorado
Front Range
J. Raton Basin
K. Uinta Basin
San Rafael Swell
L. Piceance Basin
Douglas Creek Arch
M. North Kaiparowits Plateau
Kaibab Uplift
N. San Juan Basin
Hogback Monocline
115°W
100°W
45°N
40°N
35°N
MT
WY
SD
ID
NB
UT
CO
AZ
400 km

Figure 5.

Geological Society of America Bulletin, published online on 1 February 2016 as doi:10.1130/B31431.1

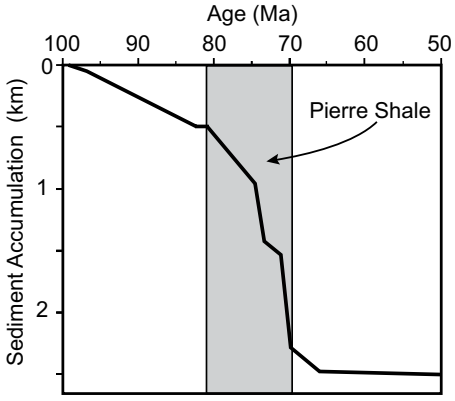

Figure 6. Sediment accumulation (burial history) from 100 to 50 Ma in the No. 1 G.W. Steiber Unit well (API 05–123–09592), Denver-Julesburg Basin. modified from Higley and Cox (2007).

records are not as tight as we would wish, mostly due to limited availability of biostratigraphic data. However, even with age uncertainties, there appears to be a general decrease in the age of initiation of Laramide deformation from southwestern Utah (ca. 78 Ma) to northeastern Wyoming (ca. 60 Ma). The results of the compilation are shown on Figure 5 for uplifts found near the sites of the subsidence analysis.

RESULTS

Observed Subsidence History

Figure 5 shows the results of our tectonic subsidence analysis of a 100 Ma–aged horizon until 50 Ma at locations in Rocky Mountain basins. In many cases, the Eocene parts of the curve are not shown. This is either because rocks of this age are missing, or because the rocks are present, but the tops of the Eocene units have not been identified, so complete thicknesses are not known.

By 100 Ma, tectonic subsidence was already in progress at a low or modest rate at all sites. Many of the curves, especially in the western part of the study area, show a marked increase in subsidence rate beginning ca. 88 Ma. This event has been noted by others (Jones et al., 2011; Liu et al., 2011; Painter and Carrapa, 2013), and some have interpreted it to denote flexural loading by either the Sevier belt to the west or early movement on nearby Laramide uplifts (Heller et al., 1986; Shuster and Steidtmann, 1988). However, this deflection is seen regionally and, within the limits of our age resolution, penecontemporaneously. These sites include those far beyond the flexural wavelength of the Sevier belt and any single Laramide uplift. So, this deflection is unlikely to be the result of flexural loading by these uplifted regions (Liu et al., 2011; Painter and Carrapa, 2013). This subsidence could have started a bit earlier or later than the 88 Ma date shown, due to the lack of detailed age constraints. At sites farther east and south, the increase in subsidence is more subdued, if present (e.g., Figs. 5B, 5C, 5J, 5M, and 5N). By ca. 80 Ma, the subsidence rates had decreased at most sites.

Subsidence accelerated again at most sites sometime between 78 Ma and 65 Ma. The magnitude and duration of this episode vary considerably from site to site. Where data on the time of initiation of the Laramide orogeny nearby are independently available, we find that it overlaps with the time of increasing basin subsidence rates in most basins (Fig. 5). In these cases, we interpret the rapid subsidence to be the result of flexural loading by nearby mountain building. The amount of subsidence everywhere between 100 Ma and the initiation of Laramide deformation is in the range of 800–1400 m. The amount of subsidence that follows initiation of Laramide deformation is more variable, with very little along the Colorado Front Range, and possibly more than 2 km in the Hanna Basin.

Somewhat anomalous features in this history are the most southeastern sites in Colorado, especially in the Denver Basin (Fig. 5I), where rapid subsidence did not commence until closer to 83–80 Ma and continued until ending ca. 70 Ma. Given that this period is confined to a single stratigraphic unit (the Pierre Shale), we have few details on possible variations of subsidence within this unit. Evidence that the subsidence rates might have varied during deposition of the Pierre Shale comes from a study of another well (Fig. 6; Higley and Cox, 2007). These variations in accumulation rates, which we assume are proxies for subsidence rates, suggest there were multiple pulses of subsidence starting a bit earlier than 80 Ma, with the last major event taking place very close to 70 Ma (Fig. 6). We suspect this compound curve may reflect multiple origins of subsidence happening around the same time at this most eastern site. The most recent pulse of subsidence at this site is coincident with the thermochronologic evidence of rapid rock uplift in the Front Range ca. 72–70 Ma (Kelley, 2002).

From the dynamic topography model, we are able to generate predicted subsidence histories for the sites where we have calculated subsidence curves. Since these predictions only include the mantle dynamic effects generated at depths below the lithosphere and do not include any shallower tectonic effects, this comparison allows us to isolate subsidence due to the tectonic effects. Consequently, this study could provide new insights on the mechanism of the Laramide orogeny.

Predicted Subsidence History Due to Dynamic Topography

In Figure 7, we present predicted dynamic topography maps from the adjoint model for specific times shown. The datum for these dynamic topography maps (Fig. 7) is an idealized global sea level. Note that these maps do not include any other effects on land surface elevation, such as isostatic perturbations within the lithosphere, erosion or deposition of the land surface, or changes in eustatic sea level. As such, relative changes in elevation are significant, but absolute elevations are not well constrained. State outlines shown on these maps have not been palinspastically restored, but this would have limited impact in our study area, east of the Sevier belt. These maps also show other observed relevant tectonic events that occurred within ±2 m.y. of the time shown. Events shown include: (1) the initiation of rapid subsidence that began after 100 Ma at the sites analyzed (Fig. 5); (2) the location of initial Laramide deformation through time (Fig. 5); (3) the locations where sheet-like conglomerates are found, as described by Heller et al. (2013), the thin, widespread bodies of which

Figure 7 (*on following page*). Maps of predicted dynamic topography of the study area and key observed geologic events from 100 to 60 Ma. Each map shows the reconstruction for time noted, but the geologic events include those taking place ±2 m.y. around the time shown. Geologic features include: the eastern apparent limit of the Cordilleran volcanic arc from North American Volcanic and Intrusive Rock Database (NAVDAT, http://www.navdat.org); the position of the approximate center of the conjugate Shatsky Rise (CSR; interpolated from Liu et al., 2010), including, for 98–88 Ma, the approximate outline of the conjugate Shatsky Rise; the initiation of Laramide deformation and the time of increase of rapid subsidence from Figure 5. Symbols are the same as in the key for Figure 8. State abbreviations: WA—Washington, OR—Oregon, UT—Utah, WY—Wyoming, CO—Colorado, CA—California, AZ—Arizona, NV—Nevada, NM—New Mexico. Locations are in north latitude and west longitude.

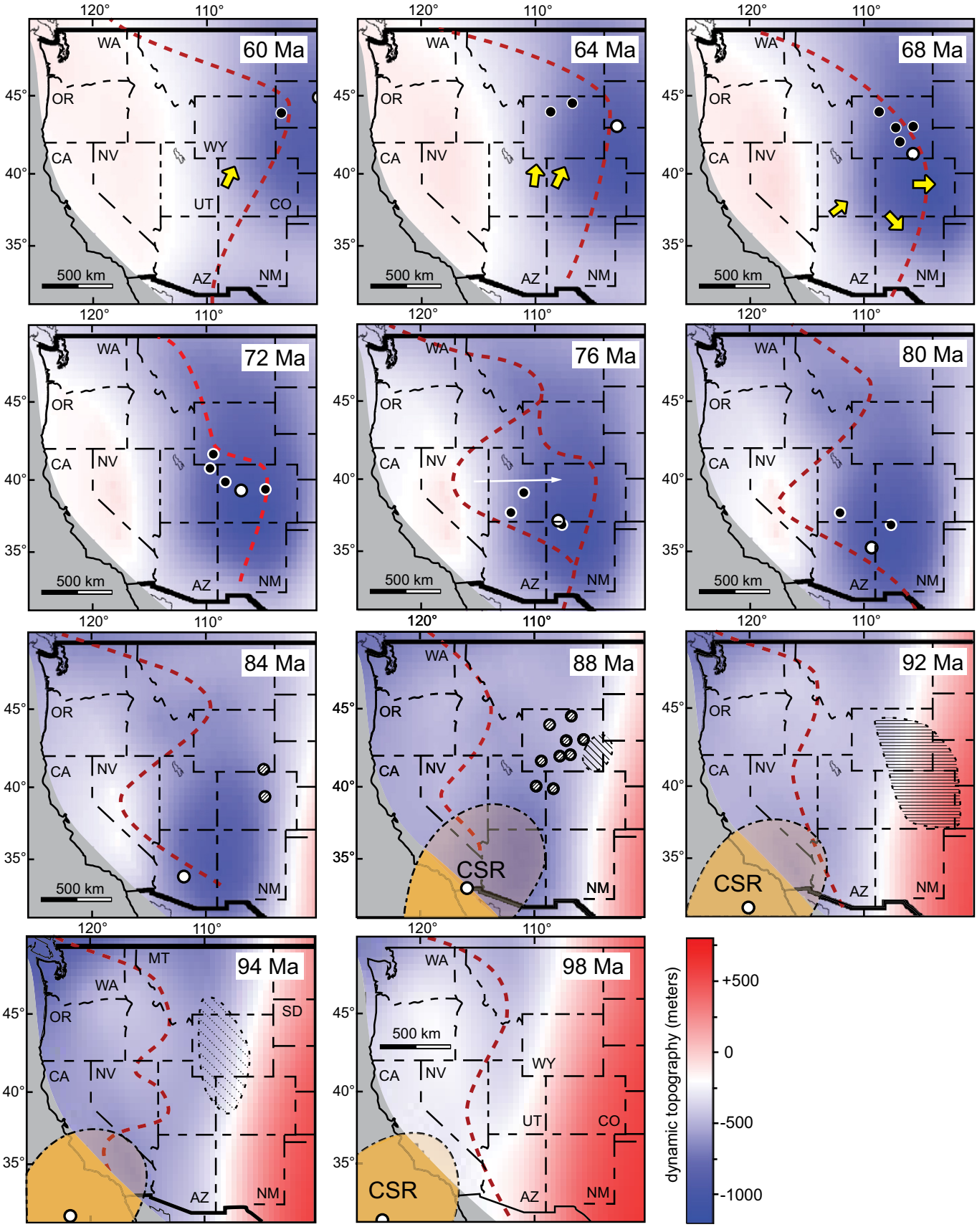
60 Ma
64 Ma
68 Ma
72 Ma
76 Ma
80 Ma
84 Ma
88 Ma
92 Ma
94 Ma
98 Ma
120°
110°
45°
40°
35°
WA
OR
CA
NV
WY
UT
CO
AZ
NM
MT
SD
500 km
CSR
dynamic topography (meters)
+500
0
-500
-1000

Figure 7.

Geological Society of America Bulletin, published online on 1 February 2016 as doi:10.1130/B31431.1

TABLE 1. DATA SOURCES ON TIME OF INITIATION OF LARAMIDE OROGENY

Basin	Type of evidence	Age range (Ma)	Reference
Bighorn Basin	Thermochronology in Beartooth Mountains	68–61	Cerveny (1990); Omar et al. (1994)
Bighorn Basin	Washakie Range fault offset and overlap	70–66	Taylor (1998)
Denver-Julesburg Basin	Thermochronology in Front Range, Colorado	71–68	Kelley (2002); Kluth and Nelson (1988)
Green River Basin	Unconformities in Ericson Formation of the Rock Springs uplift	76–72	Mederos et al. (2005)
Hanna Basin	Provenance, gravel influx in the Ferris Formation	68–60	Houston (1968); Hajek et al. (2012)
Hanna Basin	Thermochronology of Medicine Bow Range	79–60	Kelley (2005)
N. Kaiparowits Plateau	Isopach pattern, paleocurrents, fault relationships—Kaibab uplift, Circle Cliffs	80–76	Goldstrand (1994); Roberts (2007); Roberts et al. (2005, 2013); Tindall et al. (2010)
Piceance Creek Basin	Angular unconformity at top of Douglas Creek Arch	72–62	Johnson and Finn (1986); Mederos et al. (2005)
North Powder River Basin	Asymmetric isopach in basal Fort Union Formation	66–62	Ayers (1986)
South Powder River Basin	Asymmetric isopach in Lance Formation	68–66	Wang et al. (2013)
Black Hills	Fault relationships in Black Hills	ca. 60	Lisenbee and DeWitt (1993)
San Juan Basin	Asymmetric isopach in Lewis Shale	78–75	Cather (2004)
Uinta Basin	Paleocurrent shift from San Rafael Swell and erosion history	75–72	Lawton (1983)
Uinta/Piceance/Green River Basins	Conglomerate of Currant Creek Formation shed from Uinta Mountains	70–60	Bruhn et al. (1983, 1986)
Wind River	Asymmetric isopach of Lance Formation	68–66	Keefer (1970)

are interpreted to represent a change in surface tilt direction and/or magnitude resulting from regional uplift; (4) zones of major hiatus development during Cenomanian to Coniacian time from Merewether et al. (2007): although hiatuses cover large regional extents, areas shown are those of greatest duration (longest lacuna), interpreted to reflect areas of greatest erosion (Weimer, 1984; Merewether et al., 2007); (5) the inboard (eastern) limit of volcanism, assumed to be arc derived, taken from ages of intermediate volcanics on the North American Volcanic and Intrusive Rock Database (NAVDAT) Web site (Walker et al., 2006); (6) the location of collision of the conjugate Shatsky Rise based on plate reconstructions and inferred geologic evidence (Saleeby, 2003; Liu et al., 2008, 2010); and (7) the trajectory of the thickest part of the inverted fast seismic anomaly (presumably the conjugate Shatsky Rise) that generated a flat slab (Liu et al., 2010).

Predicted Temporal Changes in Dynamic Topography

Given that the elevation of land surface can be easily impacted by effects other than dynamic topography, as described earlier herein, we also show maps of average rates of change dynamic topography. These maps were derived by taking the predicted dynamic topography at a given time and subtracting from it the dynamic topography from a time 4 m.y. younger. As such, Figure 8 shows the changes in the amount of uplift/subsidence for ±2 m.y. around the times shown. These maps better show the changes in predicted surface motion over relatively short time periods that more directly influence such things as the history of basin subsidence or regional doming. For example, the map at 98 Ma in Figure 7 shows that predicted dynamic topography in the western part of the study area was low, and the eastern part was high. However, the 98 Ma map in Figure 8 shows that areas that were high were undergoing net subsidence, while the opposite was true for the areas in western Montana, where topography was the lowest (Fig. 7) but was undergoing uplift (Fig. 8). From these maps, it is easy to note regions that were undergoing uplift over 4 m.y., even if the region was below datum (blue areas on Fig. 7).

DISCUSSION

Conjugate Shatsky Rise Collision and Underflow

As described by Saleeby (2003) and Liu et al. (2010), the conjugate Shatsky Rise, if it existed, would have collided with North America in the vicinity of what is now southern California sometime between 90 and 85 Ma. Continued subduction of the conjugate Shatsky Rise would have contributed to the formation of a low-angle, flat, Farallon slab beneath the western United States. As long as the plateau remained a positively buoyant feature, it would have enhanced coupling between the two plates, resulting in shortening of the overlying plate. We assume that with continued subduction basalt in the conjugate Shatsky Rise crust would transition to eclogite, so that the feature would change from being positively to negatively buoyant. Even though the conjugate Shatsky Rise may have lost its buoyancy, the initially formed flat slab would remain in low-angle subduction due to the strong dynamic suction force (Taramón et al., 2015). Reconstructed plate motions give the Farallon slab a northeastern trajectory relative to North America, as shown by the position of the thickest part of the flat slab on Figure 7. Model results suggest that dynamic subsidence increases as slab dip angle shallows (Fig. 1C; Mitrovica et al., 1989; Liu and Gurnis, 2008), producing the map pattern seen in Figure 7. The amount of subsidence above the leading half of the conjugate Shatsky Rise is accentuated, because to the east, it would have been attached to the more steeply subducting part of the Farallon slab (Fig. 1C). The overall larger degree of negative buoyancy on the leading half of the flat slab would have generated greater dynamic subsidence.

Above the trailing half of the flat slab, subsidence quickly decreased possibly due to several processes. First, as the total thickness of the flat slab decreased, the top surface of the Farallon slab would become deeper, which reduces the magnitude of dynamic subsidence. Second, downward forces acting on the trailing part of the plateau were also less, since this part of the flat slab was farther away from the rapidly descending leading part of the subducted Farallon slab. Third, the trailing half of the flat slab may have been younger in age (Engebretson et al., 1985), resulting in reduced negative buoyancy. Finally, the possibility that this part of the basaltic crust had not yet converted to eclogite could further reduce the downward dynamic force in this part of the slab. In the extreme case, an overall buoyant lower plate might even cause isostatic uplift. This isostatic effect is not considered in our model but may explain some of the features observed on our maps.

Predicted versus Observed Subsidence History

Comparison of the predicted and observed subsidence histories shows broad, first-order consistency for the period from 100 Ma to the beginning of Laramide deformation (Fig. 5). This is not surprising given that the model includes the presence of the Western Interior Seaway as an initial constraint. Since the predicted dynamic subsidence curves are based upon long-term plate interactions coupled to relatively slow mantle flow, they only show gradual changes in vertical motion. In contrast,

Geological Society of America Bulletin, published online on 1 February 2016 as doi:10.1130/B31431.1

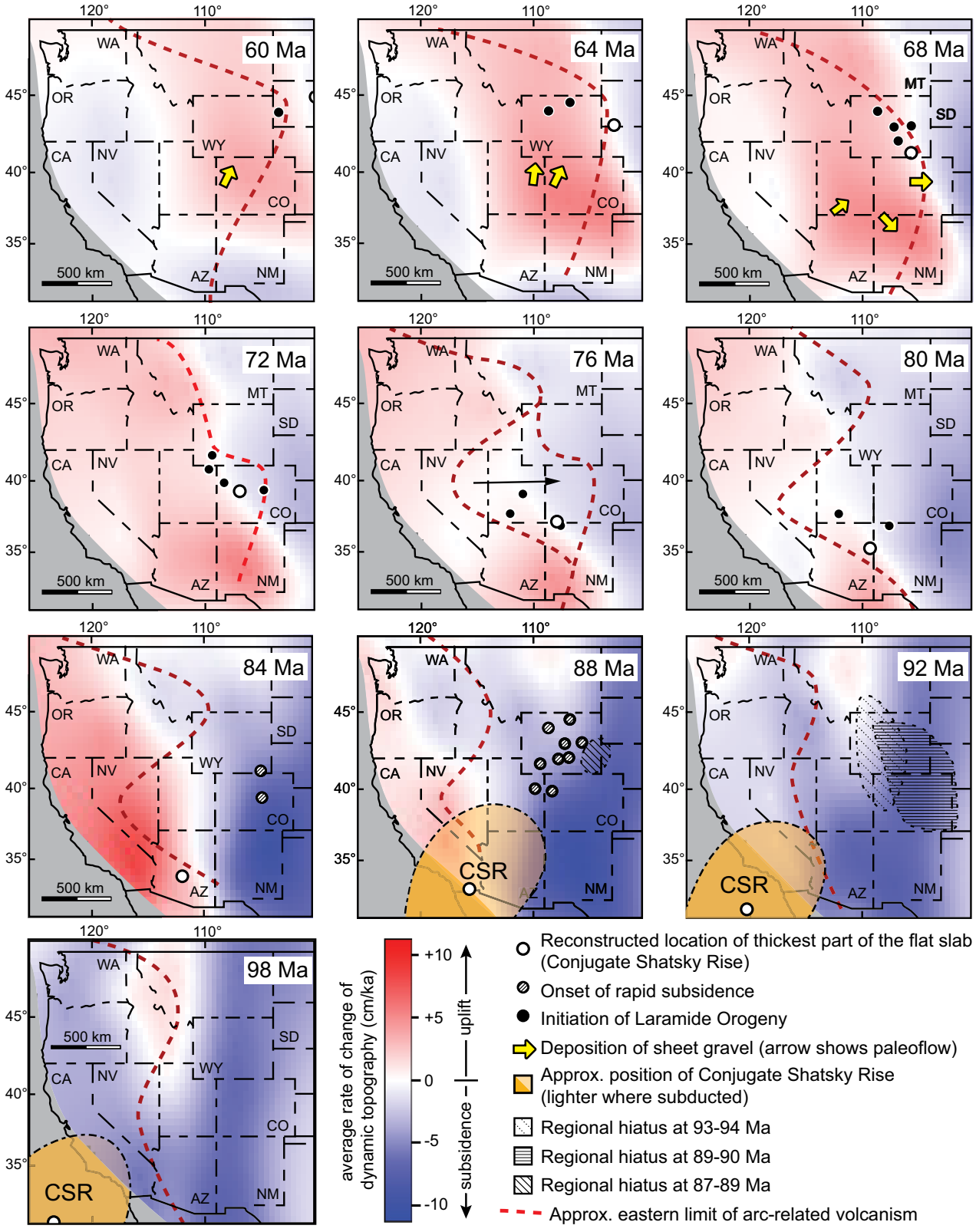

Figure 8. Time-averaged rates of subsidence/uplift from the dynamic topography model. These maps are mostly the same times as in Figure 7; however, the color bar here is average rate of change of dynamic topography (uplift vs. subsidence). These rates are averaged over 4 m.y. windows derived from comparing maps taken 2 m.y before and after the times shown. Yellow arrows show the average flow direction of widespread conglomerates discussed in text (Heller et al., 2013). CSR—conjugate Shatsky Rise. State abbreviations are the same as in Figure 7, plus MT—Montana, SD—South Dakota. Locations are in north latitude and west longitude.

Geological Society of America Bulletin, published online on 1 February 2016 as doi:10.1130/B31431.1

observed subsidence reflects not only the deep mantle origins, but also any shallower isostatic effects. In addition, the observed curves are subject to artifacts caused by: (1) any changes in eustatic sea level from 100 to 50 Ma, likely a few tens of meters (Miller et al., 2005; Cloetingh and Haq, 2015), which serves as the datum for the subsidence curves; (2) uncertainties generated by age control and regional chronostratigraphic correlations; and (3) abrupt changes of segments of the subsidence curve artificially generated by picking formation tops with no control within stratigraphic units (discussed earlier).

The model predicts on the order of 1 km of subsidence for the early parts of the curves, with more subsidence at locations farther to the east. Later on the predicted curves, all show uplift (Fig. 5) as the zone of maximum subsidence moves off to the northeast (Fig. 7). Increased subsidence to the east is the result of there being more downward force applied over time as the length of the steeply sinking Farallon slab increases with continued subduction. The amplitude and duration of early subsidence predicted by the model are broadly consistent with observed subsidence histories. For example, the predicted dynamic topography in the northern Kaiparowits region of Utah has only ~500 m of maximum subsidence with uplift beginning ca. 87 Ma, whereas the southern Powder River Basin of Wyoming has more than a kilometer of subsidence with uplift beginning ca. 65 Ma. The model predicts that subsidence rates decrease over time.

The model predicts that subsidence rates at individual wells decrease over time. Indeed, the majority of observed subsidence curves confirm this predicted decrease in subsidence rate that began earlier to the west (e.g., ca. 82 Ma in Figs. 5G and 5K) and later to the east (e.g., ca. 70 Ma in Fig. 5I). In detail, we see some mismatches. The rapid subsidence observed to start ca. 88 Ma in the western sections is later than the predicted histories suggest. We do not know if the uncertainties in the construction of all the curves can account for these mismatches. However, in any case, dynamic topography cannot explain any rapid changes in subsidence rate no matter the situation. It is possible that the apparent sharp increase in subsidence rate during the early history was dictated by the process of basalt-to-eclogite phase transformation, which is missing in the inverse-subduction model.

The major difference between predicted and observed subsidence is found in the younger parts of the curves (Fig. 5). The predicted curve shows uplift everywhere once the leading edge of the flat slab has passed beneath an area. The observed data in most locations instead show continued or accelerated subsidence. The exceptions are locations to the south and to the east in the Denver-Julesburg Basin. We ascribe this mismatch between the predicted and observed vertical motions to increased flexural subsidence caused by uplift coincident with the initiation of the Laramide orogeny. Laramide uplifts are found close to all of the sites used in our analysis. Flexural loading by the uplifts would have caused accelerated subsidence throughout all of the basins (Beck et al., 1988), although the time of onset of this subsidence will vary across the region. The rates and magnitude of subsidence will also vary with rate and size of load emplacement and proximity of the load to sites analyzed. Since our compilation shows that these late episodes of subsidence are correlative with known times of Laramide deformation, we conclude that all of these late-stage events are the record of nearby thrust loading that overwhelms any uplift that might be expected by dynamic processes.

We note that other studies have used the very rapid subsidence of the Hanna Basin (Fig. 5H) as evidence of focused subsidence by dynamic mantle processes (Cross and Pilger, 1978; Jones et al., 2011; Painter and Carrapa, 2013). Our analysis shows, instead, that the amount of dynamic subsidence in this region is no more than seen elsewhere. However, the Hanna Basin experienced unusually rapid subsidence during the Laramide orogeny. The subsidence history in the Great Divide Basin (Fig. 5D), directly adjacent to the Hanna Basin, does not show the same large magnitude of late-stage subsidence. This event is a unique and poorly understood feature of this one basin (Lillegraven et al., 2004). Both the small size of the Hanna Basin and its proximity to several Laramide ranges suggest that local three-dimensional flexural effects played more of a role in the subsidence of this basin than is seen in larger basins of the Rocky Mountains.

Vertical Motion of the Rocky Mountains

100–84 Ma

At 100 Ma, most of the Rockies sat over an area of a predicted high that lay to the east of the volcanic arc (Fig. 7). Over the subsequent 40 m.y., the topographic high migrated toward the east-northeast, followed by a zone of greatest subsidence that migrated in its wake. Once the conjugate Shatsky Rise arrived, by 85 Ma, and was subducted, the zone of greatest subsidence rates, in darkest blue on Figure 8, was centered above the leading edge of the flat slab where it was attached to the steeply dipping slab. Above the trailing edge of the flat slab, southwest of the thickest part of the conjugate Shatsky Rise (Liu et al., 2010), the region underwent gradual dynamic uplift (Fig. 8). Subsequently, as the entire flat slab began to sink into the mantle by 84(?) Ma, maximum subsidence rates abated (Fig. 8).

Between ca. 94 Ma and 87 Ma, there were regional unconformities that developed across the Rocky Mountain region. The zones of longest hiatus, shown on Figure 7, migrated from west to east as the region of greatest dynamic uplift migrated eastward. Previous studies (Weimer, 1984; Merewether et al., 2007) suggest that these unconformities resulted from eustatic sea-level changes. Here, we suggest that these features instead resulted from relative sea-level changes due to the combination of global sea level with dynamic topography. Note that the zones of greatest unconformity development track with the steepest gradient in dynamic topography from high to low, and so might be tied to surface slope more than elevation alone.

Starting around 90 Ma, the conjugate Shatsky Rise collided into the southwest United States. Following this collision, a zone of maximum subsidence developed along the trajectory of the subducted conjugate Shatsky Rise and moved to the northeast across the region that was previously high. This migration was coincident with the timing of the first maximum subsidence event seen in the curves of Figure 5. However, a pulse of increased subsidence is not observed in the southernmost sites. This may be because these areas were already undergoing rapid subsidence rates starting by 100 Ma (Fig. 8), whereas the zone of most rapid subsidence migrated to th north and east after that time. By 84 Ma, the zones of rapid subsidence shifted farther to the east, coincident with the expansion of low elevation seen in the model result (Fig. 7). Throughout most of this time period, the eastern limit of the continental arc did not migrate significantly and lay west of the zone of maximum subsidence.

84–60 Ma

From 84 to 76 Ma, the center of the conjugate Shatsky Rise migrated toward the Four Corners area of Arizona, Colorado, New Mexico, and Utah (Fig. 7). As the thickest part of the conjugate Shatsky Rise moved to the northeast, so too did the initiation of Laramide deformation and the easternmost limits of arc-related volcanism. The position of the arc front shown here includes magmatism of the Colorado Mineral Belt, which began ca. 76 Ma. This magmatism abruptly occurred much farther east of the previous arc position and was spatially restricted. As such, the Colorado Mineral Belt was likely not the simple result of migratory arc magmatism (Jones et al., 2011).

From 80 to 60 Ma, there is general coincidence among the northeastward-migrating

Geological Society of America Bulletin, published online on 1 February 2016 as doi:10.1130/B31431.1

zone of maximum dynamic subsidence, the initiation of Laramide faulting, the position of the volcanic arc front, and the center of the conjugate Shatsky Rise. This coincidence strongly suggests a coupling of all of these features. In particular, Laramide deformation began in most places where the average rate of change of dynamic topography switched from negative (subsiding) to positive (uplifting) as the thickest part of the conjugate Shatsky Rise passed through (Fig. 8). Once local Laramide deformation began, flexural loading dominated in regions near the adjacent uplifts (Fig. 5). This flexural subsidence overwhelms any regional uplift that would have been caused by dynamic topography. Farther east, beneath the western Great Plains, where there was no nearby Laramide uplift, we would predict that Paleogene uplift took place, which might help explain the scarcity of latest Cretaceous and Paleogene sedimentary rocks in that region.

From 68 to 60 Ma, as regional topography began to rise in the wake of the migrating center of subsidence, thin, sheet-like conglomerates were deposited in the central Rockies. Most of these thin conglomeratic units show a shift in paleocurrent direction to the north and/or east that suggests the region had a downward tilt in these directions (Heller et al., 2013), and these conglomerates were derived from regions of maximum uplift rate (Fig. 8).

The coincidence between the inboard limit of volcanism and the transition from areas of subsidence to areas of uplift (Fig. 8) is notable. It is not surprising to find this correlation since both arc volcanism and dynamic processes are tied to the dip and depth of the flat slab. However, since arc volcanism was not incorporated into the dynamic model, this result reaffirms interpretations that regional volcanism during Laramide time was the result of flat slab subduction.

Subsequent to the maps presented here, there was a rapid westward retreat of the arc front (Dickinson and Snyder, 1978), along with a western migration of continued Laramide deformation (Fan and Carrapa, 2014; Smith et al., 2014).

Implications for the Origin of the Laramide Orogeny

The northeastward migration of the onset of Laramide shortening at the same rate as that of North America–Farallon plate convergence strongly supports the concept that Laramide deformation was caused directly, and probably locally, by basal coupling between these plates (e.g., Lawton, 2008). In contrast, models of Laramide deformation caused by collision or other end-loading at the plate margin (Livaccari and Perry, 1993; Maxson and Tikoff, 1996; Tikoff and Maxson, 2001) would not be expected to generate this coherent, time-transgressive behavior.

Although it is impossible to know exactly the shape of the conjugate Shatsky Rise, the reconstructed Farallon slab thickness, based on seismic tomography, and timing of emplacement, based on plate motion reconstruction (Liu et al., 2010), and the geologic evidence suggest that the onset of Laramide shortening did not take place as the leading edge of the oceanic plateau moved under North America. Instead, the initiation of orogeny occurred after much of the plateau had already passed by. This might indicate that strain accumulated gradually in the upper plate prior to fault development or that, as thicker parts of the conjugate Shatsky Rise passed beneath, there was increased coupling with the overriding plate. The coincidence among the onset of Laramide deformation, the uplifting land surface in the wake of the conjugate Shatsky Rise, and the landward limit of volcanic arc activity (an indicator of slab depth) suggests that the shallowing of the Farallon slab directly contributed to the initiation of the Laramide orogeny.

As the conjugate Shatsky Rise moved under North America, it had less and less impact on the upper plate. Farther inboard, the slab was deeper, allowing less mechanical coupling with the upper plate and resulting in reduced magnitude of dynamic topography. By 60 Ma, the slab had little impact on the upper plate in generating Laramide uplifts. The youngest and most eastward Laramide uplift, the Black Hills of South Dakota, may represent the last significant direct interaction between the Farallon slab and North American plate.

CONCLUSIONS

Large-scale, low-magnitude changes in Earth topography must take place due to hydrodynamic forces generated by a viscous mantle. Dynamic topography models indicate that regions behind volcanic arcs usually experience broad subsidence. A review of the general geologic history of the western United States shows that broad, low-amplitude continental tilting existed behind the evolving Cordilleran arc throughout Mesozoic time. The low region expanded and migrated toward the east in concert with arc expansion. At a more detailed level, the predicted history of dynamic topography of the central and southern Rocky Mountains in the western United States derived from a recent adjoint inverse model compares well with our compiled history of vertical motions of the region from 100 to 50 Ma. The original dynamic model utilized seismic tomography, the known history of plate motions, and the timing and position of the Western Interior Seaway in its construction. The comparison we present includes many more details of the history of vertical movement in the western United States, including: site-specific subsidence histories, the initiation of the Laramide orogeny, and tilting of the land surface determined from the distribution of fluvial conglomerate units and regional unconformities. The predicted history of subsidence and uplift in basins of the Rocky Mountains fits the observed history well prior to the onset of the Laramide orogeny. Our results are in general agreement with those of previous studies of the likely role of dynamic topography on the formation and migration of depositional centers in the Rockies during Mesozoic time (Lawton, 1994; Liu and Nummedal, 2004; Liu et al., 2011, 2014; Heller et al., 2013; Painter and Carrapa, 2013). All of these results highlight the impact of dynamic processes in the mantle on the geologic record of surface deformation. We note that isostatic changes in elevation due to changes in lithosphere density structure and thickness likely impacted surface topography as much or more than that caused by dynamic topography, although at a smaller spatial scale. These types of changes are well known, whereas the contribution of dynamic topography generated in the mantle has been less appreciated.

In this study, we find that generally eastward-migrating areas of regional erosion are found to coincide with the passage of an area of predicted high and steep topography that migrated across the Rockies from 100 to 88 Ma. Behind this area, a zone of subsidence is predicted to have formed until ca. 60 Ma. This broad region of subsidence included a smaller zone of accelerated subsidence coincident with the northeastward migration of a hypothesized oceanic plateau, the conjugate Shatsky Rise, which helped decrease the angle of the downgoing Farallon slab. The trajectory of the conjugate Shatsky Rise and its predicted impact on dynamic topography coincide with the observed migration of accelerating subsidence seen in Rocky Mountain basins from 90 to 80 Ma. Our omission of an initially buoyant oceanic plateau crust might have led us to overpredict the amount of dynamic subsidence prior to 84 Ma.

In the wake of this migrating depocenter, a wave of uplift swept across the region until 50 Ma, following the passage of the leading edge of the flat slab. As the area rose, a wave of deformation, the Laramide orogeny, swept across the region coincident with eastward migration of the Cordilleran volcanic arc. The time-transgressive nature of the onset of Laramide deformation is consistent with localized strain

due to coupling between the Farallon and North American plates. Once deformation began, basin subsidence accelerated, likely due to flexural isostasy adjacent to Laramide uplifts. This rapid subsidence overwhelmed any impact that dynamic topography might have caused. Finally, behind the wave of initial Laramide deformation, thin, but widespread fluvial conglomeratic units were deposited in the Rocky Mountain basins of Utah, Colorado, and northwest New Mexico. These gravel units likely were derived from migrating areas of maximum uplift rate that swept across the region as the conjugate Shatsky Rise passed through.

The southwest-to-northeast migration of the initiation of the Laramide orogeny, coupled with the eastern limit of the evolving volcanic arc and the thickest part of the underlying flat slab are all consistent with the orogeny being caused by coupling between the shallowing Farallon slab and overlying North American plate. These consistencies between observations and the model predictions provide important constraints for future more detailed quantitative models aimed at understanding the lithospheric deformation of the western United States.

ACKNOWLEDGMENTS

We have benefited from discussions with William Dickinson, Ken Dueker, and Barbara John and by reviews from Timothy Lawton, Peter Copeland, and an unidentified reviewer. Partial support provided by an NSF award (1119005) to Heller.

REFERENCES CITED

Allen, P.A., Verlander, J.E., Burgess, P.M., and Audet, D.M., 2000, Jurassic giant erg deposits, flexure of the United States continental interior, and timing of the onset of Cordilleran shortening: Geology, v. 28, p. 159–162, doi:10.1130/0091-7613(2000)28<159:JGEDFO>2.0.CO;2.

Angevine, C.L., Heller, P.L., and Paola, C., 1990, Quantitative Sedimentary Basin Modeling: Tulsa, Oklahoma, American Association of Petroleum Geologists, 247 p.

Aoki, I., and Takahashi, E., 2004, Density of MORB eclogite in the upper mantle: New developments in high-pressure mineral physics and applications to the Earth's interior: Physics of the Earth and Planetary Interiors, v. 143–144, p. 129–143, doi:10.1016/j.pepi.2003.10.007.

Armstrong, R.L., and Ward, P.L., 1993, Late Triassic to earliest Eocene magmatism in the North American Cordillera: Implications for the Western Interior Basin, *in* Caldwell, W.G.E., and Kauffman, E.G., eds., Evolution of the Western Interior Basin: Geological Association of Canada Special Paper 39, p. 49–72.

Ayers, W.B., Jr., 1986, Lacustrine and fluvial-deltaic depositional systems, Fort Union Formation (Paleocene), Powder River Basin, Wyoming and Montana: American Association of Petroleum Geologists Bulletin, v. 70, p. 1651–1673.

Beck, R.A., Vondra, C.F., Filkins, J.E., and Olander, J.D., 1988, Synorogenic sedimentation and Laramide basement thrusting, Cordilleran foreland; timing of deformation, *in* Schmidt, C.J., and Perry, W.J., eds., Interaction of the Rocky Mountain Foreland and the Cordilleran Thrust Belt: Geological Society of America Memoir 171, p. 465–487, doi:10.1130/MEM171-p465.

Billen, M.I., and Gurnis, M., 2003, Comparison of dynamic flow models for the Central Aleutian and Tonga-Kermadec subduction zones: Geochemistry Geophysics Geosystems, v. 4, p. 1035, doi:10.1029/2001GC000295.

Bird, P., 1998, Kinematic history of the Laramide orogeny in latitudes 35°–49°N, western United States: Tectonics, v. 17, p. 780–801, doi:10.1029/98TC02698.

Bjerrum, C.J., and Dorsey, R.J., 1995, Tectonic controls on deposition of Middle Jurassic strata in a retroarc foreland basin, Utah-Idaho trough, western interior, United States: Tectonics, v. 14, p. 962–978, doi:10.1029/95TC01448.

Blakey, R.C., Peterson, F., and Kocurek, G., 1988, Synthesis of late Paleozoic and Mesozoic eolian deposits of the Western Interior of the United States: Sedimentary Geology, v. 56, p. 3–125, doi:10.1016/0037-0738(88)90050-4.

Bond, G., 1976, Evidence for continental subsidence in North America during the Late Cretaceous global submergence: Geology, v. 4, p. 557–560, doi:10.1130/0091-7613(1976)4<557:EFCSIN>2.0.CO;2.

Braun, J., 2010, The many surface expressions of mantle dynamics: Nature Geoscience, v. 3, p. 825–833, doi:10.1038/ngeo1020.

Bruhn, R.L., Picard, M.D., and Beck, S.L., 1983, Mesozoic and Early Tertiary Structure and Sedimentology of the Central Wasatch Mountains, Uinta Mountains, and Uinta Basin: Utah Geological Survey Special Studies 59, p. 63–105.

Bruhn, R.L., Picard, M.D., and Isby, J.S., 1986, Tectonics and sedimentology of Uinta Arch, western Uinta Mountains and Uinta Basin, *in* Peterson, J.A., ed., Paleotectonics and Sedimentation in the Rocky Mountain Region, United States: American Association of Petroleum Geologists Memoir 41, p. 333–352.

Capitanio, F., Faccenna, C., Zlotnik, S., and Stegman, D.R., 2011, Subduction dynamics and the origin of Andean orogeny and the Bolivian orocline: Nature, v. 480, p. 83–86, doi:10.1038/nature10596.

Cather, S.M., 2004, Laramide orogeny in central and northern New Mexico and southern Colorado, *in* Mack, G.H., and Giles, K.A., eds., The Geology of New Mexico—A Geologic History: New Mexico Geological Society Special Publication 11, p. 203–248.

Cerveny, P.F., 1990, Fission-Track Thermochronology of the Wind River Range and Other Basement Cored Uplifts in the Rocky Mountain Foreland [Ph.D. dissertation]: Laramie, Wyoming, University of Wyoming, 180 p.

Cloetingh, S., and Haq, B.U., 2015, Inherited landscapes and sea level change: Science, v. 347, p. 393–403, doi:10.1126/science.1258375.

Cobban, W.A., and Reeside, J.B., Jr., 1952, Correlation of the Cretaceous formations of the Western Interior United States: Geological Society of America Bulletin, v. 63, p. 1011–1043, doi:10.1130/0016-7606(1952)63[1011:COTCFO]2.0.CO;2.

Cobban, W.A., Walaszczyk, I., Obradovich, J.D., and McKinney, K.C., 2006, A USGS Zonal Table for the Upper Cretaceous Middle Cenomanian–Maastrichtian of the Western Interior of the United States Based on Ammonites, Inoceramids, and Radiometric Ages: U.S. Geological Survey Open-File Report 2006-1250, 46 p.

Coney, P.J., 1978, Mesozoic–Cenozoic Cordilleran plate tectonics: Geological Society of America, v. 152, p. 33–50, doi:10.1130/MEM152-p33.

Coney, P.J., and Reynolds, S.J., 1977, Cordilleran Benioff zones: Nature, v. 270, p. 403–406, doi:10.1038/270403a0.

Craig, L.C., Holmes, C.N., Freeman, V.L., Mullens, T.E., and Weira, G.W., 1977, Maps Showing Thickness of the Morrison Formation and Thickness and Generalized Facies of the Members of the Morrison Formation in the Colorado Plateau Region: U.S. Geological Survey Open-File Report 77-516, 5 maps.

Cross, T.A., and Pilger, R.H.J., 1978, Tectonic controls of Late Cretaceous sedimentation, Western Interior, USA: Nature, v. 274, p. 653–657, doi:10.1038/274653a0.

Dávila, F.M., and Lithgow-Bertelloni, C., 2015, Dynamic uplift during slab flattening: Earth and Planetary Science Letters, v. 425, p. 34–43, doi:10.1016/j.epsl.2015.05.026.

DeCelles, P.G., 2004, Late Jurassic to Eocene evolution of the Cordilleran thrust belt and foreland basin systems, western USA: American Journal of Science, v. 304, p. 105–168, doi:10.2475/ajs.304.2.105.

Dickinson, W.R., and Snyder, W.S., 1978, Plate tectonics of the Laramide orogeny, *in* Matthews, V., III, ed., Laramide Folding Associated with Basement Block Faulting in the Western United States: Geological Society of America Memoir 151, p. 355–366, doi:10.1130/MEM151-p355.

Dickinson, W.R., Klute, M.A., Hayes, M.J., Janecke, S.U., Lundin, E.R., McKittrick, M.A., and Olivares, M.D., 1988, Paleogeographic and paleotectonic setting of Laramide sedimentary basins in the central Rocky Mountain region: Geological Society of America Bulletin, v. 100, p. 1023–1039, doi:10.1130/0016-7606(1988)100<1023:PAPSOL>2.3.CO;2.

Engebretson, D.C., Cox, A., and Gordon, R.G., 1985, Relative Motions between Oceanic Plates of the Pacific Basin: Geological Society of America Special Paper 206, 60 p.

Erslev, E.A., 1993, Thrusts, back-thrusts, and detachments of Rocky Mountain foreland arches, *in* Schmidt, C.J., Chase, R.B., and Erslev, E.A., eds., Laramide Basement Deformation in the Rocky Mountain Foreland of the Western United States: Geological Society of America Special Paper 280, p. 339–358, doi:10.1130/SPE280-p339.

Fan, M., and Carrapa, B., 2014, Late Cretaceous–early Eocene Laramide uplift, exhumation, and basin subsidence in Wyoming: Crustal responses to flat slab subduction: Tectonics, v. 33, p. 509–529, doi:10.1002/2012TC003221.

Flament, N., Gurnis, M., and Müller, R.D., 2013, A review of observations and models of dynamic topography: Lithosphere, v. 5, p. 189–210, doi:10.1130/L245.1.

Flament, N., Gurnis, M., Williams, S., Seton, M., Skogseid, J., Heine, C., and Müller, R.D., 2014, Topographic asymmetry of the South Atlantic from global models of mantle flow and lithospheric stretching: Earth and Planetary Science Letters, v. 387, p. 107–119, doi:10.1016/j.epsl.2013.11.017.

Flowers, R.M., Wernicke, B.P., and Farley, K.A., 2008, Unroofing, incision, and uplift history of the southwestern Colorado Plateau from apatite (U-Th)/He thermochronometry: Geological Society of America Bulletin, v. 120, p. 571–587, doi:10.1130/B26231.1.

Goldstrand, P.M., 1994, Tectonic development of Upper Cretaceous to Eocene strata of southwestern Utah: Geological Society of America Bulletin, v. 106, p. 145–154, doi:10.1130/0016-7606(1994)106<0145:TDOUCT>2.3.CO;2.

Gradstein, F.M., Ogg, J.G., Schmitz, M., and Ogg, G., 2012, The Geologic Time Scale 2012: Amsterdam, Netherlands, Elsevier, 1176 p.

Grand, S.P., 2002, Mantle shear-wave tomography and the fate of subducted slabs: Philosophical Transactions of the Royal Society of London, ser. A, Mathematical and Physical Sciences, v. 360, p. 2475–2491, doi:10.1098/rsta.2002.1077.

Gurnis, M., 1993, Phanerozoic marine inundation of continents driven by dynamic topography above subducting slabs: Nature, v. 364, p. 589–593, doi:10.1038/364589a0.

Gurnis, M., Müeller, R.D., and Moresi, L., 1998, Dynamics of Cretaceous vertical motion of Australia and the Australian-Antarctic discordance: Science, v. 279, p. 1499–1504, doi:10.1126/science.279.5356.1499.

Hager, B.H., 1984, Subducted slabs and the geoid: Constraints on mantle rheology and flow: Journal of Geophysical Research–Solid Earth, v. 89, p. 6003–6015, doi:10.1029/JB089iB07p06003.

Hajek, E.A., Heller, P.L., and Schur, E.L., 2012, Field test of autogenic control on alluvial stratigraphy (Ferris Formation, Upper Cretaceous–Paleogene, Wyoming): Geological Society of America Bulletin, v. 124, p. 1898–1912, doi:10.1130/B30526.1.

Heller, P.L., Bowdler, S.S., Chambers, H.P., Coogan, J.C., Hagen, E.S., Shuster, M.W., Winslow, N.S., and Lawton, T.F., 1986, Time of initial thrusting in the Sevier orogenic belt, Idaho-Wyoming and Utah: Geology, v. 14, p. 388–391, doi:10.1130/0091-7613(1986)14<388:TOITIT>2.0.CO;2.

Heller, P.L., Dueker, K., and McMillan, M.E., 2003, Post-Paleozoic alluvial gravel transport as evidence of conti-

nental tilting in the U.S. Cordillera: Geological Society of America Bulletin, v. 115, p. 1122–1132, doi:10.1130/B25219.1.

Heller, P.L., Mathers, G., Dueker, K., and Foreman, B., 2013, Far-traveled latest Cretaceous–Paleocene conglomerates of the southern Rocky Mountains, USA: Record of transient Laramide tectonism: Geological Society of America Bulletin, v. 125, p. 490–498, doi:10.1130/B30699.1.

Higgins, P., 2003, A Wyoming succession of Paleocene mammal-bearing localities bracketing the boundary between the Torrejonian and Tiffanian North American land mammal "ages": Rocky Mountain Geology, v. 38, p. 247–280, doi:10.2113/gsrocky.38.2.247.

Higley, D.K., and Cox, D.O., 2007, Oil and gas exploration and development along the front range in the Denver Basin of Colorado, Nebraska, and Wyoming, *in* Higley, D.K., ed., Petroleum Systems and Assessment of Undiscovered Oil and Gas in the Denver Basin Province, Colorado, Kansas, Nebraska, South Dakota, and Wyoming: USGS Province 39: U.S. Geological Survey Digital Data Series DDS-69-P, 41 p.

Houston, R.S., 1968, A Regional Study of Rocks of Precambrian Age in that Part of the Medicine Bow Mountains Lying in Southeast Wyoming with a Chapter on the Relationship between Precambrian and Laramide Structure: Geological Survey of Wyoming Memoir 1, 167 p.

Hoy, R.G., and Ridgway, K.D., 1997, Structural and sedimentological development of footwall growth synclines along an intraforeland uplift, east-central Bighorn Mountains, Wyoming: Geological Society of America Bulletin, v. 109, p. 915–935, doi:10.1130/0016-7606(1997)109<0915:SASDOF>2.3.CO;2.

Johnson, R.C., and Finn, T.M., 1986, Cretaceous through Holocene history of the Douglas Creek Arch, Colorado and Utah, *in* Stone, D.S., ed., New Interpretations of Northwest Colorado Geology: Denver, Colorado, Rocky Mountains Association of Geologists, p. 77–95.

Johnson, R.C., and Johnson, S.Y., 1991, Stratigraphic and time-stratigraphic cross sections of Phanerozoic rocks along line B–B′, Uinta and Piceance Basin area, west-central Uinta Basin, Utah to eastern Piceance Basin, Colorado, U.S. Geological Survey Miscellaneous Investigations Series, I-2184-B: Washington D.C., U.S. Geological Survey, 2 sheets.

Jones, C.H., Farmer, G.L., Sageman, B., and Zhong, S., 2011, Hydrodynamic mechanism for the Laramide orogeny: Geosphere, v. 7, p. 183–201, doi:10.1130/GES00575.1.

Jones, M.A., Heller, P.L., Roca, E., Garces, M., and Cabrera, L., 2004, Time lag of syntectonic sedimentation across an alluvial basin: Theory and example from the Ebro Basin, Spain: Basin Research, v. 16, p. 489–506, doi:10.1111/j.1365-2117.2004.00244.x.

Kauffman, E.G., Sageman, B.B., Kirkland, J.I., Elder, W.P., Harries, P.J., and Villamil, T., 1993, Molluscan biostratigraphy of the Cretaceous Western Interior Basin, North America, *in* Caldwell, W.G.E., and Kauffman, E.G., eds., Evolution of the Western Interior Basin: Geological Association of Canada Special Paper 39, p. 397–434.

Keefer, W.R., 1970, Structural Geology of the Wind River Basin, Wyoming: U.S. Geological Survey Professional Paper 495-D, 35 p.

Kelley, S.A., 2002, Unroofing of the southern Front Range, Colorado: A view from the Denver Basin: Rocky Mountain Geology, v. 37, p. 189–200, doi:10.2113/gsrocky.37.2.189.

Kelley, S.A., 2005, Low-temperature cooling histories of the Cheyenne Belt and Laramie Peak shear zone, Wyoming, and the Soda Creek–Fish Creek shear zone, Colorado, *in* Karlstrom, K.E., and Keller, G.R., eds., The Rocky Mountain Region: An Evolving Lithosphere: American Geophysical Union Geophysical Monograph 54, p. 55–70, doi:10.1029/154GM05.

Kluth, C.F., and Nelson, S.N., 1988, Age of Dawson Arkose, southwestern Air Force Academy, Colorado, and implications for the uplift history of the Front Range: The Mountain Geologist, v. 25, p. 29–35.

Lawton, T.F., 1983, Late Cretaceous fluvial systems and the age of foreland uplifts in central Utah, *in* Lowell, J.D., ed., Rocky Mountain Foreland Basins and Uplifts: Denver, Colorado, Rocky Mountain Association of Geologists, p. 181–199.

Lawton, T.F., 1994, Tectonic setting of Mesozoic sedimentary basins, Rocky Mountain region, United States, *in* Caputo, M.V., Peterson, J.A., and Franczyk, K.J., eds., Mesozoic Systems of the Rocky Mountain Region: Denver, Colorado, Rocky Mountain Section, Society for Sedimentary Geology, p. 1–25.

Lawton, T.F., 2008, Laramide sedimentary basins, *in* Miall, A.D., ed., Sedimentary Basins of the United States and Canada: Sedimentary Basins of the World, Volume 5: Amsterdam, The Netherlands, Elsevier, p. 429–450, doi:10.1016/S1874-5997(08)00012-9.

Lawver, L.A., and Müller, R.D., 1994, Iceland hotspot track: Geology, v. 22, p. 311–314, doi:10.1130/0091-7613(1994)022<0311:IHT>2.3.CO;2.

Leary, R., DeCelles, P., Gehrels, G., and Morriss, M., 2015, Fluvial deposition during transition from flexural to dynamic subsidence in the Cordilleran foreland basin: Ericson Formation, western Wyoming, USA: Basin Research, v. 27, p. 495–516, doi:10.1111/bre.12085.

Lillegraven, J.A., 1993, Correlation of Paleogene strata across Wyoming—A users' guide, *in* Snoke, A.W., Steidtmann, J.R., and Roberts, S.M., eds., Geology of Wyoming: Geological Survey of Wyoming Memoir 5, p. 414–477.

Lillegraven, J.A., Snoke, A.W., and McKenna, M.C., 2004, Tectonic and paleogeographic implications of late Laramide geologic history in the northeastern corner of Wyoming's Hanna Basin: Rocky Mountain Geology, v. 39, p. 7–64, doi:10.2113/gsrocky.39.1.7.

Lisenbee, A.L., and DeWitt, E., 1993, Laramide evolution of the Black Hills uplift, *in* Snoke, A.W., Steidtmann, J.R., and Roberts, S.M., eds., Geology of Wyoming: Geological Survey of Wyoming Memoir 5, p. 374–412.

Lithgow-Bertelloni, C., and Silver, P.G., 1998, Dynamic topography, plate driving forces and the African superswell: Nature, v. 395, p. 269–272, doi:10.1038/26212.

Liu, L., 2015, The ups and downs of North America: Evaluating the role of mantle dynamic topography since the Mesozoic: Reviews of Geophysics, v. 53, no. 3, p. 1022–1049, doi:10.1002/2015RG000489.

Liu, L., and Gurnis, M., 2008, Simultaneous inversion of mantle properties and initial conditions using an adjoint of mantle convection: Journal of Geophysical Research–Solid Earth, v. 113, p. B08405, doi:10.1029/2008JB005594.

Liu, L., and Gurnis, M., 2010, Dynamic subsidence and uplift of the Colorado Plateau: Geology, v. 38, p. 663–666, doi:10.1130/G30624.1.

Liu, L., Spasojevic, S., and Gurnis, M., 2008, Reconstructing Farallon plate subduction beneath North America back to the Late Cretaceous: Science, v. 322, p. 934–938, doi:10.1126/science.1162921.

Liu, L., Gurnis, M., Seton, M., Saleeby, J., Müllwe, R.D., and Jackson, J.M., 2010, The role of oceanic plateau subduction in the Laramide orogeny: Nature Geoscience, v. 3, p. 353–357, doi:10.1038/ngeo829.

Liu, S., and Nummedal, D., 2004, Late Cretaceous subsidence in Wyoming: Quantifying the dynamic component: Geology, v. 32, p. 397–400, doi:10.1130/G20318.1.

Liu, S., Nummedal, D., and Liu, L., 2011, Migration of dynamic subsidence across the Late Cretaceous United States Western Interior Basin in response to Farallon subduction: Geology, v. 39, p. 555–558, doi:10.1130/G31692.1.

Liu, S., Nummedal, D., and Gurnis, M., 2014, Dynamic versus flexural controls of Late Cretaceous Western Interior Basin, USA: Earth and Planetary Science Letters, v. 389, p. 221–229, doi:10.1016/j.epsl.2014.01.006.

Livaccari, R.F., and Perry, F.V., 1993, Isotopic evidence for preservation of Cordilleran lithospheric mantle during the Sevier-Laramide orogeny, western United States: Geology, v. 21, p. 719–722, doi:10.1130/0091-7613(1993)021<0719:IEFPOC>2.3.CO;2.

Livaccari, R.F., Burke, K., and Sengor, A.M.C., 1981, Was the Laramide orogeny related to subduction of an oceanic plateau?: Nature, v. 289, p. 276–278, doi:10.1038/289276a0.

Manea, V., and Gurnis, M., 2007, Subduction zone evolution and low viscosity wedges and channels: Earth and Planetary Science Letters, v. 264, p. 22–45, doi:10.1016/j.epsl.2007.08.030.

Martinson, V.S., Heller, P.L., and Frerichs, W.E., 1998, Distinguishing middle Late Cretaceous tectonic events from regional sea-level change using foraminiferal data from the U.S. Western Interior: Geological Society of America Bulletin, v. 110, p. 259–268, doi:10.1130/0016-7606(1998)110<0259:DMLCTE>2.3.CO;2.

Maxson, J., and Tikoff, B., 1996, Hit-and-run collision model for the Laramide orogeny, western United States: Geology, v. 24, p. 968–972, doi:10.1130/0091-7613(1996)024<0968:HARCMF>2.3.CO;2.

McKee, E.D., 1988, Ancient sandstones considered to be eolian, *in* McKee, E.D., ed., A Study of Global Sand Seas: U.S. Geological Survey Professional Paper 1052, p. 189–238.

Mederos, S., Tikoff, B., and Bankey, V., 2005, Geometry, timing and continuity of the Rock Springs uplift, Wyoming, and Douglas Creek Arch, Colorado: Implications for uplift mechanisms in the Rocky Mountain foreland, U.S.A.: Rocky Mountain Geology, v. 40, p. 167–191, doi:10.2113/40.2.167.

Merewether, E.A., and Cobban, W.A., 1986, Biostratigraphic units and tectonism in the Mid-Cretaceous foreland of Wyoming, Colorado, and adjoining areas, *in* Peterson, J.A., ed., Paleotectonics and Sedimentation: American Association of Petroleum Geologists Memoir 41, p. 443–479.

Merewether, E.A., Cobban, W.A., and Obradovich, J.D., 2007, Regional disconformities in Turonian and Coniacian (Upper Cretaceous) strata in Colorado, Wyoming, and adjoining states—Biochronological evidence: Rocky Mountain Geology, v. 42, p. 95–122, doi:10.2113/gsrocky.42.2.95.

Miller, K.G., Kominz, M.A., Browning, J.V., Wright, J.D., Mountain, G.S., Katz, M.E., Sugarman, P.J., Cramer, B.S., Christie-Blick, N., and Pekar, S.F., 2005, The Phanerozoic record of global sea-level change: Science, v. 310, p. 1293–1298, doi:10.1126/science.1116412.

Mitrovica, J.X., Beaumont, C., and Jarvis, G.T., 1989, Tilting of continental interiors by the dynamical effects of subduction: Tectonics, v. 8, p. 1079–1094, doi:10.1029/TC008i005p01079.

Nichols, D.J., 2003, Palynostratigraphic framework for age determination and correlation of the nonmarine lower Cenozoic of the Rocky Mountains and Great Plains region, *in* Raynolds, R.G., and Flores, R.M., eds., Cenozoic Systems of the Rocky Mountain Region: Denver, Colorado, Rocky Mountain Section, Society for Sedimentary Geology, p. 107–134.

Nichols, D.J., and Fleming, R.F., 2002, Palynology and palynostratigraphy of Maastrichtian, Paleocene, and Eocene strata in the Denver Basin, Colorado: Rocky Mountain Geology, v. 37, p. 135–163, doi:10.2113/gsrocky.37.2.135.

Nichols, D.J., and Flores, R.M., 1993, Palynostratigraphic correlation of the Fort Union Formation (Paleocene) in the Wind River Reservation and Waltman area, Wind River Basin, Wyoming, *in* Keefer, W.R., Metzger, W.J., and Godwin, L.H., eds., Wyoming Geological Association Special Symposium on Oil and Gas and Other Resources of the Wind River Basin: Wyoming: Casper, Wyoming, Wyoming Geological Association, p. 175–189.

Omar, G.I., Lutz, T.M., and Giegengack, R., 1994, Apatite fission-track evidence for Laramide and post-Laramide uplift and anomalous thermal regime at the Beartooth overthrust, Montana-Wyoming: Geological Society of America Bulletin, v. 106, p. 74–85, doi:10.1130/0016-7606(1994)106<0074:AFTEFL>2.3.CO;2.

Painter, C.S., and Carrapa, B., 2013, Flexural versus dynamic processes of subsidence in the North America Cordillera basin: Geophysical Research Letters, v. 40, p. 4249–4253, doi:10.1002/grl.50831.

Peterson, J.A., 1972, Jurassic System, *in* Geologic atlas of the Rocky Mountain region United States of America: Denver, Colorado, Rocky Mountain Association of Geologists, p. 177–189.

Roberts, E.M., 2007, Facies architecture and depositional environments of the Upper Cretaceous Kaiparowits Formation, southern Utah: Sedimentary Geology, v. 197, p. 207–233, doi:10.1016/j.sedgeo.2006.10.001.

Roberts, E.M., Deino, A.L., and Chan, M.A., 2005, $^{40}Ar/^{39}Ar$ age of the Kaiparowits Formation, southern Utah, and correlation of contemporaneous Campanian strata and vertebrate faunas along the margin of the Western Interior Basin: Cretaceous Research, v. 26, p. 307–318, doi:10.1016/j.cretres.2005.01.002.

Roberts, E.M., Sampson, S.D., Deino, A.L., Bowring, S.A., and Buchwaldt, R., 2013, The Kaiparowits Formation: A remarkable record of Late Cretaceous terrestrial environments, ecosystems, and evolution in western North America, *in* Titus, A.L., and Loewen, M.A., eds., At the Top of the Grand Staircase: The Late Cretaceous of Southern Utah: Life of the Past: Bloomington, Indiana, Indiana University Press, p. 85–106.

Saleeby, J.B., 2003, Segmentation of the Laramide slab—Evidence from the southern Sierra Nevada region: Geological Society of America Bulletin, v. 115, p. 655–668, doi:10.1130/0016-7606(2003)115<0655:SOTLSF>2.0.CO;2.

Saleeby, J.B., Farley, K.A., Kistler, R.W., and Fleck, R.J., 2007, Thermal evolution and exhumation of deep-level batholithic exposures, southernmost Sierra Nevada, California, *in* Cloos, M., Carlson, W.D., Gilbert, M.C., Liou, J.G., and Sorenson, S.S., eds., Convergent Margin Terranes and Associated Regions: A Tribute to W.G. Ernst: Geological Society of America Special Paper 419, p. 39–66, doi:10.1130/2007.2419(02).

Schwartz, R.K., and DeCelles, P.G., 1988, Cordilleran foreland basin evolution in response to interactive Cretaceous thrusting and foreland partitioning, southwestern Montana, *in* Schmidt, C.J., and Perry, W.J., Jr., eds., Interaction of the Rocky Mountain Foreland and the Cordilleran Thrust Belt: Geological Society of America Memoir 171, p. 489–513, doi:10.1130/MEM171-p489.

Scott, R.W., 2014, A Cretaceous chronostratigraphic database: Construction and applications [Notebooks on Geology]: Carnets de Géologie, v. 14, p. 15–37.

Shuster, M.W., and Steidtmann, J.R., 1988, Tectonic and sedimentary evolution of the northern Green River Basin, western Wyoming, *in* Schmidt, C.J., and Perry, W.J., eds., Interaction of the Rocky Mountain Foreland and the Cordilleran Thrust Belt: Geological Society of America Memoir 171, p. 515–530, doi:10.1130/MEM171-p515.

Smith, A.D., 2007, A plate model for Jurassic to recent intraplate volcanism in the Pacific Ocean basin, *in* Foulger, G.R., and Jurdy, D.M., eds., Plates, Plumes and Planetary Processes: Geological Society of America Special Paper 430, p. 471–495, doi:10.1130/2007.2430(23).

Smith, A.G., Smith, D.G., and Funnel, B.M., 1994, Atlas of Mesozoic and Cenozoic Coastlines: New York, Cambridge University Press, 99 p.

Smith, M.E., Carroll, A.R., Jicha, B.R., Cassel, E.J., and Scott, J.J., 2014, Paleogeographic record of Eocene Farallon slab rollback beneath western North America: Geology, v. 42, p. 1039–1042, doi:10.1130/G36025.1.

Steckler, M.S., and Watts, A.B., 1978, Subsidence of the Atlantic type continental margin off New York: Earth and Planetary Science Letters, v. 41, p. 1–13, doi:10.1016/0012-821X(78)90036-5.

Steidtmann, J.R., and Middleton, L.T., 1991, Fault chronology and uplift history of the southern Wind River Range, Wyoming: Implications for Laramide and post-Laramide deformation in the Rocky Mountain foreland: Geological Society of America Bulletin, v. 103, p. 472–485, doi:10.1130/0016-7606(1991)103<0472:FCAUHO>2.3.CO;2.

Stevenson, D.J., and Turner, J.S., 1977, Angle of subduction: Nature, v. 270, p. 334–336, doi:10.1038/270334a0.

Taramón, J.M., Rodríguez-González, J., Negredo, A.M., and Billen, M.I., 2015, Influence of cratonic lithosphere on the formation and evolution of flat slabs: Insights from 3-D time-dependent modeling: Geochemistry Geophysics Geosystems, v. 16, p. 2933–2948, doi:10.1002/2015GC005940.

Taylor, D.J., 1998, Processing and interpretation of 2-D seismic data from the Bighorn Basin, Wyoming, *in* Keefer, W.R., and Goolsby, J.E., eds., Cretaceous and Lower Tertiary Rocks of the Bighorn Basin, Wyoming and Montana: Wyoming Geological Association Guidebook 49, p. 179–196.

Tikoff, B., and Maxson, J., 2001, Lithospheric buckling of the Laramide foreland during Late Cretaceous and Paleogene, western United States: Rocky Mountain Geology, v. 36, p. 13–35, doi:10.2113/gsrocky.36.1.13.

Tindall, S.E., Storm, L.P., Jenesky, T.A., and Simpson, E.L., 2010, Growth faults in the Kaiparowits Basin, Utah, pinpoint initial Laramide deformation in the western Colorado Plateau: Lithosphere, v. 2, p. 221–231, doi:10.1130/L79.1.

van Hinte, J.E., 1978, Geohistory analysis—Application of micropaleontology in exploration geology: American Association of Petroleum Geologists Bulletin, v. 62, p. 201–222.

Walker, J.D., Bowers, T.D., Black, R.A., Glazner, A.F., Farmer, G.L., and Carlson, R.W., 2006, A geochemical database for western North American volcanic and intrusive rocks (NAVDAT), *in* Sinha, A.K., ed., Geoinformatics: Data to Knowledge: Geological Society of America Special Paper 397, p. 61–71, doi:10.1130/2006.2397(05).

Wang, S., Heller, P.L., Jones, N.R., and Fan, M., 2013, Flexural modeling of Laramide basins in Wyoming: A test of paleoaltimetric and rigidity estimates: Geological Society of America Abstracts with Programs, v. 45, no. 7, p. 669.

Weimer, R.J., 1984, Relation of unconformities, tectonics, and sea-level changes, Cretaceous of Western Interior, U.S.A., *in* Schlee, J.S., ed., Interregional Unconformities and Hydrocarbon Accumulation: American Association of Petroleum Geologists Memoir 36, p. 7–35.

Wyoming Geological Association Stratigraphic Committee, 2014, Wyoming Stratigraphic Nomenclature Chart: Casper, Wyoming, Wyoming Geological Association, 1 sheet.

Xu, W., Lithgow-Bertelloni, C., Stixrude, L., and Ritsema, J., 2008, The effect of bulk composition and temperature on mantle seismic structure: Earth and Planetary Science Letters, v. 275, p. 70–79, doi:10.1016/j.epsl.2008.08.012.

Yonkee, A., and Weil, A.B., 2015, Tectonic evolution of the Sevier and Laramide belts within the North American Cordillera orogenic system: Earth-Science Reviews, v. 150, p. 531–593.

Science Editor: Christian Koeberl
Associate Editor: Timothy Lawton

Manuscript Received 24 September 2015
Revised Manuscript Received 21 December 2015
Manuscript Accepted 7 January 2016

Printed in the USA

Geological Society of America Bulletin

Dynamic topography and vertical motion of the U.S. Rocky Mountain region prior to and during the Laramide orogeny

Paul L. Heller and Lijun Liu

Geological Society of America Bulletin published online 1 February 2016;
doi: 10.1130/B31431.1